The Journal of Chemical Physics ARTICLE scitation.org/journal/jcp

Reorientation-induced Stokes shifts caused by directional interactions in electronic spectroscopy: Fast dynamics of poly(methyl methacrylate)

Cite as: J. Chem. Phys. 150, 194201 (2019); doi: 10.1063/1.5094806
Submitted: 5 March 2019 • Accepted: 24 April 2019 •
Published Online: 16 May 2019

Joseph E. Thomaz, Patrick L. Kramer, Sebastian M. Fica-Contreras, David J. Hoffman, and Michael D. Fayer[a)]

AFFILIATIONS

Department of Chemistry, Stanford University, Stanford, California 94305, USA

[a)]fayer@stanford.edu. **Tel.:** 650 723-4446.

ABSTRACT

Dynamic Stokes shift measurements report on structural relaxation, driven by a dipole created in a chromophore by its excitation from the ground electronic state to the S_1 state. Here, we demonstrate that it is also possible to have an additional contribution from orientational relaxation of the Stokes shift chromophore. This effect, called reorientation-induced Stokes shift (RISS), can be observed when the reorientation of the chromophore and the solvent structural relaxation occur on similar time scales. Through a vector interaction, the electronic transition of the chromophore couples to its environment. The orientational diffusive motions of the chromophores will have a slight bias toward reducing the transition energy (red shift) as do the solvent structural diffusive motions. RISS is manifested in the polarization-dependence of the fluorescence Stokes shift using coumarin 153 (C153) in poly(methyl methacrylate) (PMMA). A similar phenomenon, reorientation-induced spectral diffusion (RISD), has been observed and theoretically explicated in the context of two dimensional infrared (2D IR) experiments. Here, we generalize the existing RISD theory to include properties of electronic transitions that generally are not present in vibrational transitions. Expressions are derived that permit determination of the structural dynamics by accounting for the RISS contributions. Using these generalized equations, the structural dynamics of the medium can be measured for any system in which the directional interaction is well represented by a first order Stark effect and RISS or RISD is observed. The theoretical results are applied to the PMMA data, and the structural dynamics are obtained and discussed.

I. INTRODUCTION

Dynamic Stokes shift measurements observed through time-dependent fluorescence spectroscopy have been historically used, and simulated, to investigate solvent response in a variety of different chemical systems such as molecular solvents,[1–3] ionic liquids (ILs),[4–7] nanoconfined fluids,[8–11] and sensitized nanoparticles.[12–14] Stokes shift probes function via a dipole change caused by excitation of the $S_0 \rightarrow S_1$ transition. The alteration in dipole induces the surrounding medium to undergo structural changes to accommodate modified interactions with the new dipole. The perturbation to the chemical environment is small, so linear response theory applies,[15] and the surrounding system will still relax through equilibrium fluctuations. In this technique, the solvent relaxation is manifested as a time-dependent Stokes shift. Upon excitation, the fluorescence emission will be centered at the frequency $\nu(t = 0)$. As solvation occurs, the emission red shifts until equilibrium in the excited state has been achieved, and the final emission frequency is $\nu(t = \infty)$.

In simple low viscosity molecular liquids, complete solvation will typically occur within a matter of picoseconds. More viscous and complex systems, such as ionic liquids, may take up to several nanoseconds for complete structural relaxation to occur. The same approach can be used to study dynamics in polymers. While

the aspects of polymer dynamics, such as long distance diffusion of polymer chains, are incredibly slow, and therefore, outside the experimental time window of fluorescence spectroscopy, as shown in this work, fluorescence Stokes shift measurements can report on faster structural motions, which can be important in various processes. In other techniques used for the study of polymer dynamics, such as dielectric spectroscopy or thermal conductivity,[16–19] it can be difficult or impossible to observe fast polymer dynamics as they will be overwhelmed by slower polymer dynamics. A few ultrafast measurements of polymers have been conducted;[20–22] however, these techniques all measure the femtosecond to the picosecond regime and do not extend from picoseconds to nanoseconds and tens of nanoseconds.

In this paper, we present a time-dependent Stokes shift study of the dynamics of poly(methyl methacrylate) (PMMA) using coumarin 153 (C153) as the probe. The experiments show a substantial polarization-dependence, that is, the time-dependence of the Stokes shift depends on the polarization of the fluorescence that is observed. The time-dependent Stokes shift can be related to the frequency-frequency correlation function (FFCF), which is also measured by other techniques such as two dimensional infrared (2D IR) spectroscopy,[23] hole burning,[24] and transient absorption.[25] It is well know that the steady state emission spectrum depends on the FFCF.[25] Therefore, it is reasonable that the dynamic Stokes shift is also related to the FFCF.[25–27] A rigorous derivation of the relationship between the dynamic Stokes shift and the FFCF is given in the Appendix.

A polarization-dependence of dynamic observables has been observed in 2D IR experiments. Specifically, in 2015, reorientation-induced spectral diffusion (RISD) was first observed and characterized through 2D IR utilizing the O–D stretch of methanol-d_4 as the vibrational probe in a room temperature ionic liquid.[28,29] The spectral diffusion of the probe displayed a clear dependence on the relative polarizations of the pulses used in the experiments. The probe orientational relaxation occurred on times comparable to the liquid structural dynamics. Because the probe was coupled to the medium though the 1st order vibrational Stark effect, the reorientation of the probe was responsible for part of the observed spectral diffusion. The reorientation-induced spectral diffusion (RISD) contribution to the total spectral diffusion depends on the polarizations used in the experiment. Since then these effects have been observed several times,[30–33] and the theory has been expanded upon to include 2nd order Stark effects,[34,35] and RISD in nonisotropic distributions of the probe molecule.[36]

There have been a number of rigorous studies of Stokes shift probes in molecular and ionic liquids,[4–6,37] and some have considered the possibility of polarization-dependence,[8,37,38] yet a polarization-dependence has not been observed. It has been pointed out that this effect might be possible, but it was not observed in the particular studies.[8,37,38] In one instance, it was explicitly stated that a polarization-dependence was not observed because the probe orientational relaxation occurred much more slowly than the solvation, which has been the case for low and moderate viscosity molecular solvents.[1] The data presented below show that the time-dependent Stokes shift may differ when the fluorescence is observed parallel and perpendicular to the excitation polarization. The presence of a polarization-dependence indicates that there are two separate factors contributing to the observable: structural

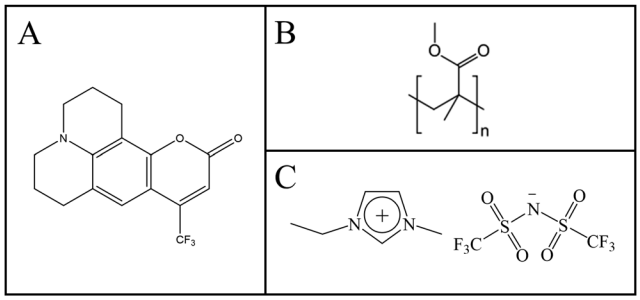

FIG. 1. Relevant molecular structures to the study: (a) 2,3,6,7-Tetrahydro-9-(trifluoromethyl)-1*H*,5*H*,11*H*-[1]benzopyrano(6,7,8-ij)quinolizin-11-one, or coumarin 153, the fluorescent probe. (b) Poly(methyl methacrylate) (PMMA), the studied polymer at a molecular weight of 350k. (c) 1-Ethyl-3-methylimidazolium bis(trifluoromethylsulfonyl)imide (EmimNTf$_2$), an ionic liquid well studied through dynamic Stokes shift used as a control not demonstrating any polarization dependence.

Stokes shifts (SSSs) and reorientation-induced Stokes shifts (RISSs). Since the dynamic Stokes shift measurements are reflective of the FFCF, this phenomenon is related to the RISD model applied to the 2D IR experiments.[28–36] The RISD model is reconsidered and generalized to accommodate factors that can be important for fluorescence probes but not vibrational probes, specifically angle differences between the difference dipole and the absorption transition dipole and the possible angle difference between the absorption and emission dipoles. As with the RISD theory, the RISS theory enables the separation of the dynamic data into SSS and RISS components. The RISS contribution to the Stokes shift is completely determined by measurement of the orientational relaxation of the C153 probe chromophore. Then using a simultaneous global fit of the observed parallel, perpendicular, and isotropic dynamic Stokes Shift measurements, the desired SSS is obtained from the data. For comparison, the same experimental procedures were followed using C153 in the ionic liquid 1-ethyl-3-methylimidazolium bis(trifluoromethylsulfonyl)imide (EmimNTf$_2$), and no polarization dependence was observed.[7,8] The molecular structures are given in Fig. 1.

This experimental and theoretical study presents the first observation of RISS and expands upon the existing theory that describes it. The theory allows the SSS to be separated from the RISS, which permits time-dependent Stokes shift measurements to examine polymer structural dynamics on fast to moderate time scales. As shown below, the presence of RISS can actually aid in the determination of the SSS as there are multiple time-dependent datasets that contain the same structural dynamics.

II. MATERIALS AND METHODS

Methyl methacrylate (monomer) was purchased from TCI America and used without further purification. PMMA (polymer) was purchased from Sigma at an average molecular weight of 350 000 verified by gel permeation chromatography. C153 was purchased from TCI America at 98% purity. Samples for the fluorescence experiments were prepared such that the final concentration of C153 was 10^{-3}M. Polymer samples were solvent cast using chloroform

directly on a fused silica substrate producing a 50 μm film. The resulting film was pumped under vacuum (100 mTorr) for 4 days to remove residual solvent. While under vacuum, PMMA samples were heated above their glass transition. Due to the hygroscopic nature of PMMA, samples remained under vacuum and were placed in a nitrogen filled glovebox where the sample cell was assembled. The sample was held between crossed polarizers showing no signs of depolarization. $EmimNTf_2$ ionic liquid (IL) was ordered from IoLiTec at 99% high purity (HP) grade. The IL was placed under vacuum and dried for one week at a temperature of 60 °C. It was determined with coulometric Karl Fischer titration that the water content was below 30 ppm. It has been shown that changes in ionic liquid properties are negligible for water content less than 100 ppm.[39] Due to its hygroscopic nature, the IL was stored in a glovebox, and all further sample preparation was conducted in a glovebox.

Fluorescence solvation dynamics experiments were conducted utilizing time correlated single photon counting (TCSPC). A Ti:sapphire oscillator producing approximately 100 fs laser pulses at an wavelength of 730 nm was employed. This wavelength was frequency doubled through second harmonic generation (SHG) in a β-barium borate (BBO) crystal to 365 nm for excitation of C153. The bandwidth of the 365 nm excitation pulse was 5.8 nm. The laser repetition rate was lowered from 80 MHz to 5 MHz using an acousto-optic single pulse selector. A computer-controlled half wave plate rotated the excitation beam polarization so the measurements could be made parallel, perpendicular, and at the magic angle (isotropic) relative to a polarizer with fixed polarization mounted at the entrance slit of a monochromator. The sample was excited from the front surface in a near-normal geometry through a hole in the lens that collected the fluorescence. A second lens imaged the fluorescence onto the monochromator entrance slit. The fluorescence was frequency resolved by the monochromator, and single photons were detected with a multichannel plate (MCP) detector at wavelengths ranging from 400 nm to 600 nm in increments of 5 nm.

The instrument response was obtained by measuring the fluorescence lifetime of aqueous acidified malachite green with an optical density matching that of the sample, under identical experimental conditions to the sample measurements. Malachite green has an extremely short fluorescence lifetime, 5 ps, which is short compared to the instrument response.[40] Measurement of its fluorescence lifetime on this system gives the instrument response including the effects of the finite thickness of the sample cell. The instrument response was no greater than 70 ps full width at half maximum.

Data were collected at each emission wavelength for 15 s. The wavelength scans were repeated until it was determined that an acceptable signal-to-noise level had been reached. After one full sweep of the wavelength range, the excitation polarization was changed. Fluorescence data were taken at parallel, perpendicular, and isotropic (magic angle) polarizations relative to the resolving polarizer into the monochromator. Once all three polarizations were taken, the sample was moved to a new spot on the PMMA sample using a motorized stage. All data were taken with the same entrance slit width, and all other experimental conditions were identical so that the relative amplitude at each emission wavelength was correct.

Polarized steady state spectra were taken on a Horiba FluoroLog Fluorimeter with built-in excitation and emission polarizers. The excitation polarizer was rotated relative to the emission polarizer to measure parallel and perpendicular polarization to match the ultrafast experiments. Steady state samples were excited at 365 nm, and emissions were collected from 400 nm to 600 nm in increments of 1 nm.

III. RESULTS AND DISCUSSION

A. Ultrafast spectra comparison

The Stokes shift dynamics following the excitation of C153 to the S_1 state in both PMMA and $EmimNTf_2$ were observed by collecting the excited state population decay curves measured with parallel, perpendicular, and isotropic (magic angle) polarization configurations at emission wavelengths ranging from 600 nm to 400 nm in 5 nm increments. In energy units, this corresponds to a range of 2.066 eV–3.010 eV incremented by 0.023 eV. The observable in this technique is the emission peak center as a function of time. Figure 2(a) displays isotropic fluorescence decays of C153 in PMMA

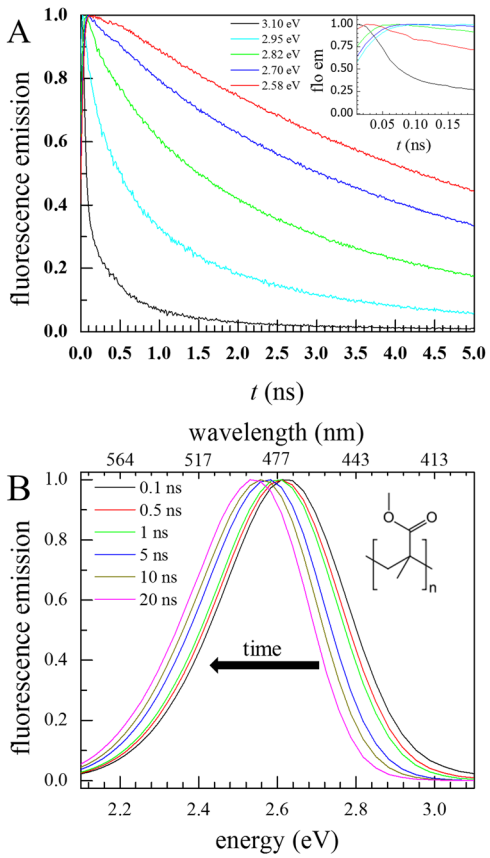

FIG. 2. (a) Representative emission decays collected via TCSPC. For this experiment, emissions were collected from 400 nm to 600 nm in increments of 5 nm. In energy units, this corresponds to a range from 2.07 eV to 3.10 eV. (b) Dynamic Stokes shift emission measurements at select representative times.

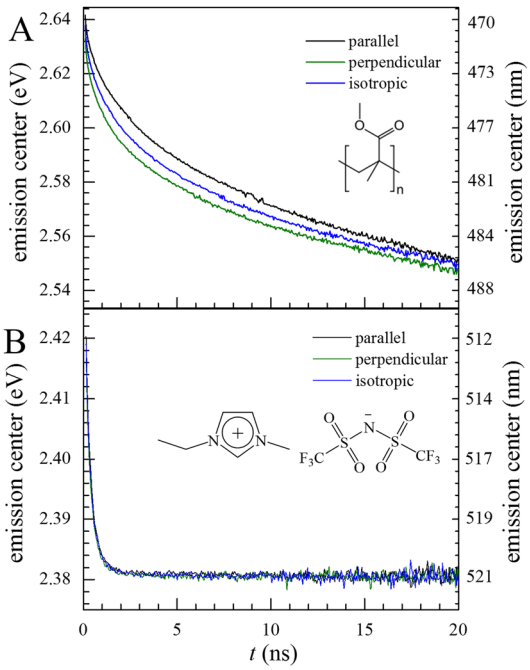

FIG. 3. Parallel, perpendicular, and isotropic dynamic Stokes shift measurements of C153 in (a) $EmimNTf_2$ and (b) PMMA. As with the steady state spectra, distinct differences are observed in the case of C153 PMMA as opposed to C153 in $EmimNTf_2$ where any difference is negligible.

on a semilog plot at several representative frequencies. The characteristic behavior of the fluorescence decay of a Stokes shift probe is observed. On the blue side of the emission peak, there is an initial fast decay as the spectrum shifts away from the observation wavelength, while on the red side of the line, there is an initial growth in fluorescence intensity as the spectrum shifts toward the observation wavelength. Figure 2(b) shows a sample of the data collected on C153 in PMMA at various time slices ranging from 100 ps to 20 ns. As time increases, the spectra shift to the red with the band shape remaining essentially constant.

From the time-dependent fluorescence emission shown in Fig. 2(b), as well as the parallel and perpendicular counterparts, one can track the Stokes shift over time. Although the fluorescence emission is often described as a log-normal distribution, near the maximum of the emission, the data fit well to a single Gaussian. Therefore, each time slice was fit to a Gaussian with a fit range defined by ±0.1 eV (±20 nm) centered on the highest amplitude of the emission spectrum. Figure 3 shows the plots for PMMA [Fig. 3(a)] and $EmimNTf_2$ [Fig. 3(b)] emission centers as functions of time for each polarization. In PMMA, a substantial polarization-dependence is observed. The isotropic data shown in Fig. 3 were collected as an independent magic angle measurement. However, the same curve can be constructed by adding the emission curves of parallel plus 2 times perpendicular, demonstrating the reliability of the data. It is evident that there is no polarization-dependence in $EmimNTf_2$. Regardless of polarization, previously published solvation dynamics are recovered.[8] In $EmimNTf_2$, the observed dynamics report exclusively on the structural dynamics of the ionic liquid. Table I shows the time constants and final frequencies of biexponential fits to the data in Fig. 3. In PMMA, the time constants from parallel and perpendicular vary up to 25%. These time constants vary because there are two separate contributions to the Stokes shift, i.e., structural Stokes shift (SSS) and reorientation induced Stokes shift (RISS). The RISS contribution is polarization-dependent.

Figure 4(a) is a cartoon illustrating the two contributions to the observed dynamics. Dynamic Stokes shift measurements are generally interpreted as caused by time-dependent solvent reorganization that is the response to the change in the dipole of the chromophore upon excitation. These dynamics occur in PMMA and the SSS is indeed one of the major contributors to the observed dynamic Stokes shift. However, in PMMA and similar systems, the probe orientational relaxation occurs on the same time scales as the solvent relaxation. The reorientation of the probe also causes a time-dependent Stokes shift.

A polarization-dependence has previously been observed and theoretically described for spectral diffusion measured in 2D IR experiments. The polarization-dependence of the time-dependence of the spectral diffusion occurs if the vibrational probe's intermolecular interactions with the medium are vectorial in nature, e.g., the Stark effect, and if the probe orientational relaxation occurs on the same time scales as the structural spectral diffusion (SSD) [see Fig. 4(b)].[28,29] For the Stark effect, as the probe rotates in a slowly varying electric field produced by the medium, the Stark coupling changes, which changes the probe's vibrational frequency. This change in frequency contributes to the spectral diffusion (RISD).

TABLE I. Biexponential fits to solvation dynamics parameters of C153 in $EmimNTf_2$ and PMMA. Biexponential fits to C153 in PMMA and $EmimNTf_2$. No polarization dependence was observed in $EmimNTf_2$, and all curves fit to the same time constants. PMMA isotropic was taken as an independent dataset at the magic angle; however, a near identical trace can be constructed by tracking the emission maximum of parallel plus two times perpendicular.

	τ_1 (ns)	τ_2 (ns)	$\nu(\infty)$ (eV)
PMMA parallel	1.16 ± 0.03	13.89 ± 0.33	2.533 ± 0.000 8
PMMA perpendicular	0.92 ± 0.03	11.84 ± 0.24	2.536 ± 0.000 5
PMMA isotropic	0.98 ± 0.03	11.80 ± 0.24	2.538 ± 0.000 5
$EmimNTf_2$	0.13 ± 0.02	0.41 ± 0.02	2.380 ± 0.000 04

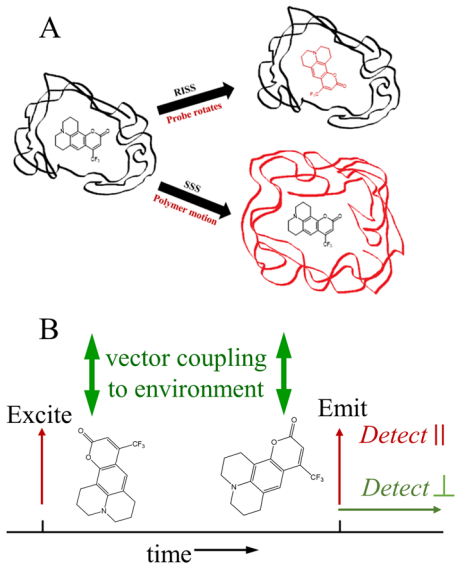

FIG. 4. (a) A cartoon highlighting the difference between RISS and SSS. In the case of RISS, the spectrum shifts as a result of probe rotation while the surroundings remain the same. In SSS, the spectrum shifts because the probe surroundings are reorganizing to accommodate the probe's induced dipole. It should be explicitly noted that the motions are coupled and occurring simultaneously. (b) Illustration of the RISS process for a fluorescent probe molecule, C153. Upon excitation, the molecule experiences a slowly evolving electric field. Rotation of the molecule changes both the orientation of the difference dipole moment relative to the electric field and the absorption and emission transition dipoles relative to the laser field polarizations, changing both the emission frequency and the molecule's contribution to the observed signal. The contribution of the frequency change to parallel emission relative to the initial excitation is reduced, while the contribution to perpendicular emission relative to the initial excitation is increased. For the magic angle or isotropic average, all frequency changes due to rotation contribute equally.

The contribution of RISD to the spectral diffusion depends on the relative polarizations of the pulses in the 2D IR pulse sequence.

The RISS also requires a vectorial coupling between the probe chromophore (C153) and the PMMA medium. The vector coupling is inherent in the Stokes shift experiment. The excitation to S_1 produces a change in the magnitude and/or direction of the dipole vector. It is this change in the vector interactions with the medium that causes the medium to respond. In addition to the structural changes of the medium, the C153 undergoes orientational relaxation [see Fig. 4(b)]. As the chromophore changes its orientation, it changes its interactions with the surrounding polymer. These alterations in intermolecular interactions cause the frequency of the S_0 to S_1 transition to change. However, while the reorientation is caused by thermal fluctuations, it is not completely random. There is a slight bias in the orientational random walk toward lower energy. Therefore, the reorientation produces a contribution to the Stokes shift. This contribution has not been seen previously because the SSS in systems studied is much faster than the orientational relaxation. In this study of PMMA, the orientational relaxation and the SSS are on overlapping time scales, so the RISS is manifested.

The RISS produces the polarization-dependence of the Stokes shift decays shown in Fig. 3(a). For parallel polarization, the fluorescence is detected with the same polarization as the excitation. Reorientation causes RISS, but as the ensemble of initially excited chromophores rotates, the molecules move away from the parallel direction and contribute less and less to the observed signal even as the contribution to the frequency change increases. In contrast, for perpendicular polarization, the fluorescence is detected with the polarization perpendicular to the excitation [see Fig. 4(b)]. Again, orientational motions contribute to the frequency change, but as the ensemble of initially excited chromophores undergoes orientational relaxation, it contributes more and more to the signal. Therefore, RISS has a larger effect on the perpendicular signal than on the parallel signal. For both polarization configurations and for the isotropic decay, the contribution of SSS is the same. As presented below, and as derived in complete detail in Sec. IV, the SSS and RISS can be separated, providing the desired information on the structural dynamics of the PMMA medium. RISS is, in principle, present in all Stokes shift experiments, but when the SSS is much faster than the orientational relaxation of the chromophore, the Stokes shift is complete before RISS can contribute.

B. Steady state spectra comparison

The time-dependent data shown in Fig. 3(a) clearly demonstrates the presence of a polarization-dependence. It is also possible to observe the polarization-dependence in steady state fluorescence spectra. In Fig. 5, the parallel and perpendicular steady state spectra of C153 in PMMA and C153 in $EmimNT_2$ are shown. The PMMA spectra in Fig. 5(a) show that the entire perpendicular spectrum is red shifted from the parallel spectrum. In the $EmimNTf_2$ spectra shown in Fig. 5(b), there is no peak shift and the two spectra are virtually identical.

The steady state fluorescence spectrum is a weighted average of the emission over the fluorescence lifetime. As shown in Fig. 3(a), the Stokes shift is not complete in 20 ns. The fluorescence lifetime of C153 in PMMA is 5.6 ns (see below). As discussed above and shown in Fig. 3(a), the perpendicular polarization has a faster Stokes shift than the parallel polarization to the same final shift because the RISS contribution to the Stokes shift is faster for perpendicular observation. Because the steady state fluorescence spectrum is not a spectrum of the fully relaxed system, the faster perpendicular Stokes shift is manifested in the perpendicular polarization spectrum as the observed red shift. In fact, even if the final frequency is reached within the experimental window, it is still possible to observe polarization-dependence in the steady state spectrum because early time data are weighted more heavily as a result of the exponential decay of the fluorescence.

In the field of time-dependent Stokes shifts, a common method of data analysis is to collect all emission wavelengths independently, optimizing the count rate at each emission wavelength, and weight them to an unpolarized steady state spectrum. In the case of simple solvents where there are fast dynamics and no polarization-dependence, this method is accurate. However, if there is a polarization-dependence, it is not sufficient. While the spectra in Fig. 5 are similar, amplitudes can vary by as much as 12% in some regions. In addition, the red and blue sides of the spectrum would be weighted improperly in opposite directions leading

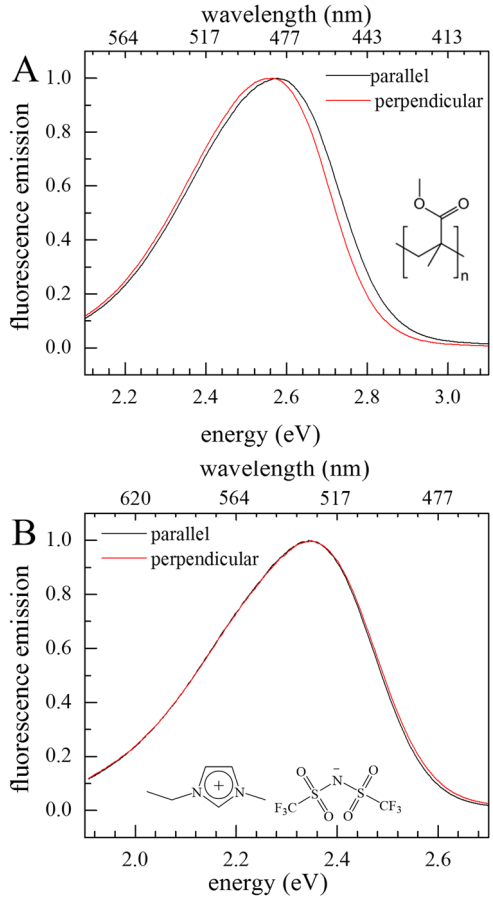

FIG. 5. Polarized steady state fluorescence spectra of C153 in (a) PMMA and (b) $EmimNTf_2$. Perpendicular was collected by rotation of the excitation polarizer to match the time-dependent experiment. In the case of PMMA, a distinct shift in the steady state spectra is observed. This is due to the presence of a polarization dependence.

to further issues in the data analysis. Therefore, it is useful to test a sample by comparing the polarization-dependence of the steady state spectra. If there is a polarization-dependence, it is an indication that RISS is contributing to the Stokes shift data, and the data collection method described above should be implemented to use the separation technique presented below.

C. Anisotropy comparison

To obtain the SSS by separating it from the RISS, it is necessary to measure the orientational relaxation of the probe chromophore. In previous solvation dynamics studies, it has been common practice to report the orientational dynamics of the Stokes shift probe by collecting parallel and perpendicular fluorescence emissions at a single wavelength. It should be noted that in many of these studies, the authors explicitly made sure that there was no variance in sample anisotropy across the emission band before reporting their findings.[8,37,38] In the case of C153 in PMMA, and other samples exhibiting polarization-dependent solvation, collecting the anisotropy decays at a single emission wavelength will introduce errors. The proper manner to collect anisotropies is to integrate the entire emission spectrum at each time point and polarization, removing any effects of dynamic Stokes shift from the data. The excited state population decay (lifetime) can also be obtained using this integration method.

From the frequency integrated parallel and perpendicular decays

$$I_{\parallel}^{\text{int}}(t) = \int I_{\parallel}(t,\omega)\,\mathrm{d}\omega = P(t)(1 + 0.8C_2(t))/3 \tag{1a}$$

and

$$I_{\perp}^{\text{int}}(t) = \int I_{\perp}(t,\omega)\,\mathrm{d}\omega = P(t)(1 - 0.4C_2(t))/3, \tag{1b}$$

the anisotropy decays were able to be calculated independently of the effects of the Stokes shift. They still, however, depend on the excited state population decay and orientational relaxation. The excited state population decay is given here by

$$P(t) = \int I_{\text{iso}}(t,\omega)\,\mathrm{d}\omega = I_{\text{iso}}^{\text{int}}(t) = I_{\parallel}^{\text{int}}(t) + 2I_{\perp}^{\text{int}}(t), \tag{2}$$

and the anisotropy, $r(t)$, is given by

$$r(t) = \frac{I_{\parallel}^{\text{int}}(t) - I_{\perp}^{\text{int}}(t)}{I_{\parallel}^{\text{int}}(t) + 2I_{\perp}^{\text{int}}(t)} = 0.4C_2(t). \tag{3}$$

$C_2(t)$ is the 2nd order Legendre polynomial orientational correlation function. The denominator in Eq. (3) removes the population contribution, so $r(t)$ decays due to pure rotational dynamics. The anisotropy begins from 0.4 for perfect orientational correlation and then decays to a final value of zero for randomized orientations.

The anisotropy and excited state population decay of C153 in PMMA are shown in Fig. 6. The solvation dynamics presented in these measurements were removed through the spectrum integration and affect neither anisotropy nor population. C153 has a single exponential excited state population decay in both $EmimNTf_2$ and PMMA [Fig. 6(b)], with fluorescence lifetimes of 6.0 ns and 5.6 ns, respectively. Neither of their orientational relaxations decay as single exponentials. Although complete orientational relaxation is achieved in both the PMMA and $EmimNTf_2$, a multiexponential anisotropy decay for a single ensemble (demonstrated by the single exponential population decays) is indicative of restricted orientational relaxation on shorter time scales followed by complete orientational randomization after all orientational constraints have been relaxed. The wobbling-in-a-cone model is used to analyze the nonexponential anisotropy decays.[41–44] In the wobbling-in-a-cone description, orientational relaxation occurs initially by free diffusion over a restricted angular range, the cone. Constraint release, as the surroundings fluctuate, allows further angular sampling, in this case a larger cone, followed finally by complete orientational randomization.

In Fig. 6, it can be seen that the anisotropy decay of C153 in PMMA starts well below the theoretical maximum of 0.4. This effect is caused by inertial (ballistic) motions of the chromophore that occur too fast to be observed on the experimental time scale; sampling of the inertial cone is complete well within the instrument response time. However, the difference between 0.4 and the observed initial values of the data can be used to quantify the angular range

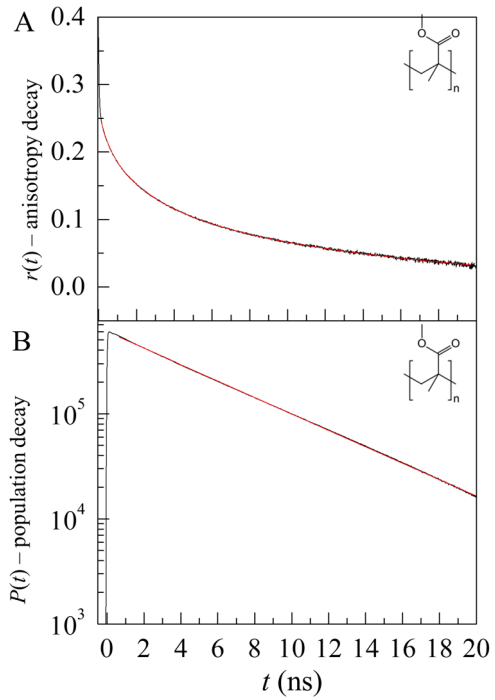

FIG. 6. (a) Integrated anisotropy of C153 in PMMA. These were collected by performing the typical anisotropy equation integrating the parallel and perpendicular emission spectra rather than a single emission in order to remove any bias from RISS. (b) Integrated isotropic fluorescence emission extracts a single population of C153 in PMMA. The excited state lifetime is 5.6 nm.

sampled on a time scale short compared to the instrument response. In the case of an inertial cone (short time angular sampling) and then two slower time scale wobbling cones, $C_2(t)$ can be modeled as[45]

$$C_2(t) = (1 - S_{\text{in}}^2)e^{-t/\tau_{\text{in}}} + S_{\text{in}}^2\left(S_{c1}^2 + (1 - S_{c1}^2)e^{-t/\tau_{c1}}\right) \times \left(S_{c2}^2 + (1 - S_{c2}^2)e^{-t/\tau_{c2}}\right)e^{-t/\tau_m}. \quad (4)$$

In Eq. (4), S_i, S_{c1}, and S_{c2} are order parameters describing the restricted motions experienced by the probe, where i is for inertial and c is for the wobbling cone.[46] Wobbling causes the anisotropy to decay to a plateau. The amplitude of the plateau is determined by the cone angle. Then, the next component causes further decay to another plateau. The final complete orientational relaxation takes the anisotropy to zero. τ_{in} is the time constant of the ultrafast inertial component, τ_{ck} is the wobbling time constant for the kth cone, and τ_m is the total orientational randomization time constant. τ_{in} is too fast to measure, and in the analysis, the first term of Eq. (4) is assumed to have decayed to zero before the first data point. Only the order parameter (cone angle) can be obtained: S_{in}^2 sets the initial value of the second term. τ_{ck} and τ_m are obtained by fitting the anisotropy data to a triexponential function. The slowest component is τ_m and corresponds to total orientational randomization of the probe. The order parameter can be used to obtain the cone angle,

$$S_k^2 = \left(\frac{\cos\theta_k(1 + \cos\theta_k)}{2}\right)^2, \quad (5)$$

where θ_k is the cone half angle of the kth cone.

Utilizing the wobbling model, one can separate the restricted (cone) motions from the total reorientation. For both solvents, an inertial cone was observed. C153 in PMMA displays two diffusive cones [an effectively triexponential data decay, Eq. (4)], while in EmimNTf$_2$ there is one diffusive cone. For the EmimNTf$_2$ analysis, S_{c2} can be taken to be 1, so the other terms with subscripts c_2 can be dropped. The wobbling-in-a-cone and complete orientational randomization parameters for C153 in both systems are displayed in Table II. The relationship between the reorientation times and RISS is discussed in detail below.

D. Solvation component separation and interpretation

The anisotropy data yield $C_2(t)$, from which $C_1(t)$ and $C_3(t)$, the first and third Legendre correlation functions, can be constructed. These are necessary to implement the RISS analysis. The expressions presented below and derived in Sec. IV differ from a related theory that described reorientation induced spectral diffusion (RISD) used in the analysis of 2D IR experiments performed on vibrational probes.[28–35] The RISD theory is expanded to account for two features of fluorescence Stokes shift probes that generally do not arise for vibrational spectral diffusion probes. First, the absorption transition dipole and the difference dipole induced by the electronic excitation do not necessarily lie along the same axis. The angle between the transition dipole and the difference dipole is denoted ψ. Second, the absorption and emission transition dipoles may not lie along the same axis. The angle between the absorption and emission transition dipoles is denoted δ. The expressions for the time-dependence of the fluorescence Stokes shift that includes both RISS and SSS are

TABLE II. Wobbling-in-a-cone analysis of orientational dynamics of C153 in PMMA and EmimNTf$_2$. Wobbling-in-a-cone analysis was run on the anisotropy decays of C153 in PMMA and EmimNTf$_2$. Theta values correspond to half cone angles in order to quantify restricted motions. EmimNTf$_2$ is well modeled as having a single inertial cone and a single diffusive cone, while PMMA was modeled using a single inertial cone and two diffusive cones.

	Θ_{in}	Θ_{c1}	Θ_{c2}	τ_{c1} (ns)	τ_{c2} (ns)	τ_m (ns)
PMMA	30.2 ± 0.1	19.4 ± 0.2	32.1 ± 0.1	0.50 ± 0.03	2.80 ± 0.07	14.07 ± 0.07
EmimNTf$_2$	27.6 ± 0.2	19.6 ± 0.1	. . .	0.28 ± 0.01	. . .	2.01 ± 0.01

$$S_{\parallel}(t) = \frac{\mathrm{SSS}(t)}{75(1+(4/5)P_2(\cos\delta)C_2(t))} \times \begin{bmatrix} C_1(t)[75+12P_2(\cos\delta)(1+P_2(\cos\psi))] \\ +C_2(t)[20P_2(\cos\delta)(1-P_2(\cos\psi))] \\ +C_3(t)[4P_2(\cos\delta)(7+2P_2(\cos\psi))] \end{bmatrix}, \quad (6)$$

$$S_{\perp}(t) = \frac{\mathrm{SSS}(t)}{75(1-(2/5)P_2(\cos\delta)C_2(t))} \times \begin{bmatrix} C_1(t)[75-6P_2(\cos\delta)(1+P_2(\cos\psi))] \\ -C_2(t)[10P_2(\cos\delta)(1-P_2(\cos\psi))] \\ -C_3(t)[2P_2(\cos\delta)(7+2P_2(\cos\psi))] \end{bmatrix}, \quad (7)$$

$$S_{\mathrm{iso}}(t) = \mathrm{SSS}(t) \times C_1(t), \quad (8)$$

with P_2, the second Legendre polynomial, given by

$$P_2(\cos(x)) = \frac{\left(3\cos(x)^2 - 1\right)}{2}. \quad (9)$$

The $SSS(t)$ is the time dependent structural Stokes shift. Equations (6)–(8) show that the structural Stokes shift, which is the property that has been measured in previous time-dependent Stokes shift experiments and corresponds to the solvent reorganization, can be obtained. The anisotropy measurements directly give $C_2(t)$ from the second order Legendre orientational correlation polynomial, $C_2(t)$, extracted from the anisotropy, the first and third order Legendre orientational correlation polynomials $C_1(t)$ and $C_3(t)$ can be constructed. Therefore, the time-dependent terms of the RISS component of the Stokes shift are known from a separate measurement of the anisotropy decay [see Fig. 6(a)]. It is possible to measure δ and ψ with independent experiments or they can be used as adjustable parameters when fitting the data. The δ and ψ are constants associated with the molecular transition; therefore, the values must be the same in all Stokes shift expressions using the chromophore. It should be noted that for a vibrational probe in which the angles δ and ψ become relevant, Eqs. (6)–(8) should be used rather than the previously published RISD equations.[28,29] The physical underpinning for a vibrational transition or an electronic transition coupling to their environments is identical. RISS is a generalization of the RISD theory. A full derivation of the RISS theory yielding Eqs. (6)–(8) is given in Sec. IV.

For C153 used here, it has been reported that there is negligible difference between the absorption and emission dipoles moment angles, i.e., $\delta = 0$.[1] In the present study, the angle between the absorption transition dipole and the difference dipole was initially included as a free parameter. However, it consistently converged to 0 in the fits; fixing it to any other value made the fits to the data worse. Therefore, for C153, Eqs. (6) and (7) reduce to the RISD equations previously presented in 2D IR, and Eq. (8) is always independent of the δ and ψ, and the same as the isotropic RISD equation.[28,29]

Using the above fitting functions, simultaneous global fits of all three polarizations of the dynamic Stokes shift of C153 in PMMA were performed. The data and the fits are shown in Fig. 7(a). The final frequency of the PMMA was determined to be 2.538 eV (488.5 nm), very close to the final Stokes shift of C153 in the methyl methacrylate monomer (2.530 eV). It is important to note that in

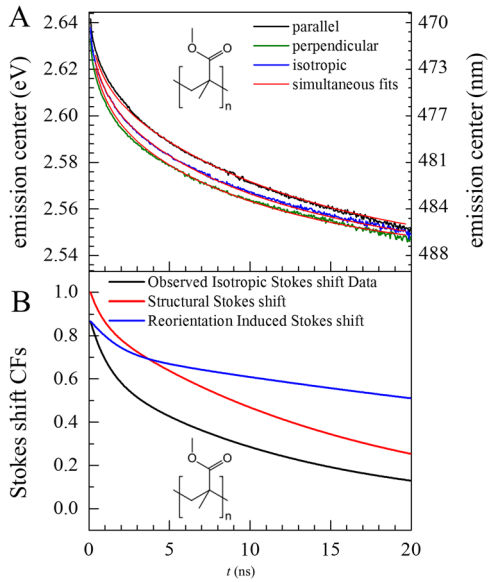

FIG. 7. (a) Fits using the RISS model to the dynamic Stokes shift data of C153 in PMMA. The same parameters were used to fit all three polarizations as well as the anisotropy [Fig 7(a)] to a high degree of accuracy. (b) The SSS and RISS of C153 in PMMA compared to the observed isotropic dynamic Stokes shift. The significant shift of the RISS trace in the first 5 ns highlights that it is the wobbling component of the orientational dynamics that are responsible for the manifestation of a polarization dependence in the data.

Eqs. (7)–(9), the time-dependence of all three Legendre polynomials was determined from the anisotropy measurements, so these are not adjusted in the fits. The $SSS(t)$, the structural Stokes shift, is a biexponential for C153 in PMMA and is polarization independent. With δ and ψ both equal to zero, there are the same number of shared parameters in the three fitting functions as the number of free parameters that would be used to fit a simple biexponential. The SSS parameters are given in Table III. To quantify how much of an effect RISS actually had on the observed decays, the fractional contribution of the SSS in the isotropic data was calculated

$$\langle k_i \rangle = 1/\langle \tau_i \rangle = \frac{\sum_n a_{i,n}}{\sum_n a_{i,n}\tau_{i,n}}, \quad (10)$$

$$\Lambda_{SSS} = \frac{\langle k_{SSS} \rangle}{\langle k_{SSS} \rangle + \langle k_{RISS} \rangle}. \quad (11)$$

$\langle k_i \rangle$ is the average rate constant, and Λ_{SSS} is the fractional component of SSS in the total Stokes shift. Structural changes accounted for 77% of the observed isotropic Stokes shift. It is important to recognize that this $\langle k_{RISS} \rangle$ will vary with polarization while $\langle k_{SSS} \rangle$ does not. The isotropic signal, $S_{\mathrm{iso}}(t) = S_{\parallel}(t) + 2S_{\perp}(t)$, given by Eq. (9) was used because it is independent of δ and ψ, so the RISS factor is $C_1(t)$.

Figure 7(b) shows the observed dynamic Stokes shift, the SSS, and the RISS. The SSS component was normalized using the traditional Stokes shift correlation function (SSCF),

$$S(t) = \frac{\nu(t) - \nu(\infty)}{\nu(0) - \nu(\infty)}, \quad (12)$$

TABLE III. Separated Structural Stokes (SSS) shift components of C153 in PMMA. Structural Stokes shift (SSS) components, amplitudes, and time constants, separated from the reorientation-induced components. The SSS corresponds to the solvent reorganization to accommodate the induced dipole. Average rate constants ($\langle k_i \rangle$) were also calculated for the structural and reorientation-induced components of the Stokes shifts. The fractional component of SSS in the total Stokes shift (Λ_{SSS}) was calculated to show how much of the observed dynamics was structural. This value can vary from 0 to 1.

A_{SSS1}	τ_{SSS1} (ns)	A_{SSS2}	τ_{SSS2} (ns)	$\nu(\infty)$ (eV)	$\langle k_{SSS} \rangle$ (ns^{-1})	$\langle k_{RISS} \rangle$ (ns^{-1})	Λ_{SSS}
0.15 ± 0.01	0.87 ± 0.06	0.85 ± 0.01	16.24 ± 0.18	2.538 ± 2 × 10^{-4}	0.072 ± 0.001	0.021 ± 0.001	0.77

and the other two curves have initial values consistent with the SSS component. Since the SSS value is 1 at $t = 0$, and the data are SSS × RISS, the RISS and the data will have the same $t = 0$ values. The experimental isotropic dynamic Stokes shift will be faster than its SSS and RISS components unless there is no RISS contribution, in which case the observed dynamic Stokes shift is purely SSS. Figure 7(b) shows that RISS can have a significant effect on the experimental Stokes shift data, particularly at early time. Therefore, to obtain the SSS(t) correctly, it is necessary to consider the possibility of a contribution from RISS(t). RISS will be important when at least a component of the orientational relaxation of the chromophore occurs on the time scale of the SSS. It is not necessary for complete randomization of the chromophore to occur more quickly than solvation. For the isotropic data [Eq. (9)], the RISS is determined solely by $C_1(t)$. For single exponential orientational relaxation, the decay of $C_1(t)$ is a factor of 3 slower than $C_2(t)$, which is measured in the anisotropy experiments. In the expressions for the parallel and perpendicular data [Eqs. (7) and (8)], $C_1(t)$ is the dominant term. Returning to the data for EmimNTf$_2$ (Fig. 3), there is no polarization-dependence that can be observed within the noise. However, in Tables I and II, the wobbling component of the orientational relaxation is somewhat faster than the slow component of the observed Stokes shift. However, the vast majority of the Stokes shift occurs faster than the fast component of the orientational relaxation. In addition, since $C_1(t)$ dominates RISS(t), the main contribution to RISS is slower than the small amplitude slow component of the Stokes shift data. Therefore, RISS is not observed within the noise of the experiment.

While the presence of RISS is a complication for extracting the structural dynamics from the Stokes shift data, it can also be useful. Because of the limitation imposed by the fluorescence lifetime, it was not possible to observe the Stokes shift data taken in PMMA go to the final frequency, $\nu(\infty)$ [see Fig. 3(a)], which is a necessary input into the SSCF [Eq. (12)]. With a single curve that does not decay to a constant value as it does in the EmimNTf$_2$ data [Fig. 3(b)], it is difficult to determine $\nu(\infty)$. However, because the sample is isotropic, the three curves shown in Fig. 3(a) must all have the same $\nu(\infty)$. Therefore, in the global fit with the value of $\nu(\infty)$ shared in fitting the three curves, an accurate value of $\nu(\infty)$ can be obtained.

Table III gives the SSS decay time constants for the PMMA. One is just under a nanosecond and the other is about 16 ns. These are the time scales for structural motions that occur in response to the perturbation created by excitation of C153. Clearly there are vastly slower motions in PMMA, e.g., the diffusion of polymer chains. At room temperature, PMMA is deep in the glass state, so these whole chain motions will occur on macroscopic time scales. The observed times must reflect the motion of smaller, more local moieties that comprise the polymer PMMA, in particular, is known to have a major secondary relaxation that appears on microsecond time scales.[47] This motion has been associated with PMMA's ester side chain, and many of PMMA's favorable mechanical properties[48,49] and long-term aging behavior[50] have been attributed to its existence. Less studied, extremely localized relaxations comprising only parts of the side chain are sometimes reported in dynamic mechanical analysis studies,[51] and may provide a still better match for the nanosecond time scale of the observed dynamic.

IV. THEORY

A. Separation of reorientation induced Stokes shift from structural dynamics

The SSCF, Eq. (12), determines the dynamic Stokes shift of fluorescence emission and is equivalent to the (normalized) FFCF of electronic absorption frequencies that is responsible for line shapes observed in both steady-state and time-resolved nonlinear spectroscopies.[23,25,52,53] A full derivation of this relationship is available in the Appendix. In the evaluation of the correlation function average, it is commonly assumed that an isotropic ensemble is used when the sample environment is isotropic, such as in a liquid or amorphous solid. However, when the spectroscopic technique for measuring these correlation functions utilizes (linearly) polarized laser pulses, the ensemble of molecules generating the signal is not isotropic. Each pair of interactions between a linearly polarized laser electric field and molecular transition dipole (i.e., absorption or emission of a photon) preferentially samples a subset of molecules according to a cosine-squared angular distribution of these transition dipoles.

The polarization-selectivity that results from exciting and probing nonuniform distributions is frequently used to measure molecular orientational relaxation dynamics through the anisotropy decay with both time-resolved fluorescence and pump-probe methodologies.[25,52,54] Recent experimental and theoretical work in ultrafast infrared spectroscopy has revealed another consequence of polarization-selective excitation and probe interactions: correlation functions of molecular quantities having a vector or directional nature appear different depending on the relative laser field polarizations used in the experiment.[28,29,34] In measurements of the FFCF from time-dependent 2D IR line shapes, a vibrational frequency fluctuation determined (in part) by the orientational relaxation

of the molecule results in reorientation-induced spectral diffusion (RISD) that changes in form depending on the polarization configuration of the experiment. The FFCF measured in the all-parallel configuration, $\langle ZZZZ \rangle$, is slower than the isotropic average, while that measured for the perpendicular configuration, $\langle ZZXX \rangle$, is faster. The influence of RISD can be determined from the known orientational relaxation dynamics of the probe by evaluating the FFCF in a polarization-weighted ensemble.[28]

In this section, we extend the theory of RISD[28,29] to account for several differences in the photophysics of probe molecules undergoing electronic energy level transitions, compared to the vibrational transitions considered previously. The results will be appropriate for the analysis of both reorientation-induced Stokes shift (RISS) for fluorescent probe molecules and RISD which could potentially be observed in 2D electronic spectroscopy (2D ES) analogous to 2D IR. Figure 4(b) is a simple illustration of the fluorescence probe interaction with vectorial coupling leading to the manifestation of RISS. To make the derivation concrete, we will take the vector interaction to be the first order Stark effect, although any first order vectorial coupling (based on a vector dot product) will give the same results with a different interpretation for the numerical quantities appearing.

Excitation of an electronic transition in a Stokes shift probe molecule, e.g., C153, results in a large change in the molecular dipole moment. We define the difference in dipole moment, a vector quantity, by $\Delta\vec{\mu} = \langle e|\vec{\mu}|e\rangle - \langle g|\vec{\mu}|g\rangle$, with g denoting the ground state, e denoting the excited state, and $\vec{\mu}$ denoting the dipole operator. Although the value of $\Delta\vec{\mu}$ is a quantum mechanical result, we can operate with it as a classical quantity because it involves expectation values. The first order Stark effect gives a change in observed transition frequency of

$$\Delta\omega = \omega - \omega_0 = -\Delta\vec{\mu}\cdot\vec{E} \tag{13}$$

through the interaction of this difference dipole with the total electric field $\vec{E}$ evaluated at the location of $\Delta\vec{\mu}$.[55–57] Here, ω is the observed absorption frequency and ω_0 is the molecular frequency in the absence of the electric field produced by the medium.

We write the electric field as $\vec{E} = E\times\hat{e}$, where E is the field magnitude and $\hat{e}$ is the unit vector specifying its direction, and likewise the difference dipole as $\Delta\vec{\mu} = \Delta\mu\times\hat{\mu}_D$, with $\Delta\mu$ being the difference dipole magnitude and $\hat{\mu}_D$ being its unit vector. Then, the Stark shift takes the form

$$\Delta\omega = -\Delta\mu E\hat{\mu}_D\cdot\hat{e} = -\Delta\mu E\cos(\theta_{\mathrm{FD}}), \tag{14}$$

where θ_{FD} is the angle between the electric field and difference dipole unit vectors.

At this point, we introduce the first coordinate system, called the field frame. In this frame, the field unit vector $\hat{e}$ corresponds to the z-axis, called Z_{F}, and is shown at an arbitrary position in the lab frame (X_{L}, Y_{L}, Z_{L}) in Fig. 8. Equation (14) can be interpreted as giving the dependence of the Stark shift on the orientation of the difference dipole vector in the field frame. The only significant angle is the polar angle θ_{FD}, though, in general, we can define a difference dipole frame with Euler angles $\Omega_{\mathrm{FD}} = (\phi_{\mathrm{FD}}, \theta_{\mathrm{FD}}, \chi_{\mathrm{FD}})$ relative to the field frame. The convention for angular coordinates, their subscripts, and transformations here is that FD represents a transformation of the system (the difference dipole frame, denoted D) *from* coincidence with the field frame (denoted F) *to* its current orientation (D).

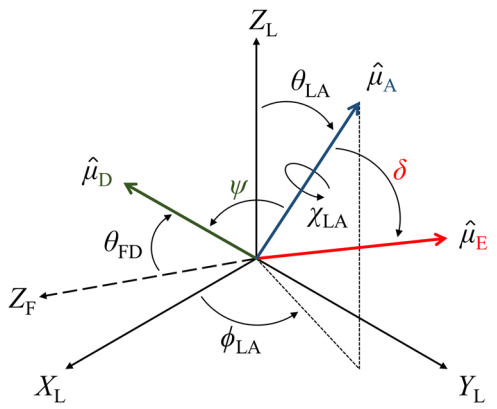

FIG. 8. Schematic of angles characterizing the fluorescent probe molecule used in calculating the frequency shift due to a first order Stark effect and the resulting polarization-weighted RISS factors. The Euler angles (ϕ_{LA}, θ_{LA}, χ_{LA}) give the orientation of the molecular frame in the lab frame, defined such that the absorption transition dipole $\hat{\mu}_{\mathrm{A}}$ is parallel to the molecular z-axis. The angles between $\hat{\mu}_{\mathrm{A}}$ and the emission transition dipole, $\hat{\mu}_{\mathrm{E}}$, and the difference dipole moment, $\hat{\mu}_{\mathrm{D}}$, are δ and ψ, respectively. The electric field frame z-axis is shown, with angle θ_{FD} to the difference dipole moment. Both the field frame and molecular frame positions (Euler angles) relative to the lab frame will evolve in time due to fluctuations in the material.

We take $\Delta\mu$ to be a constant of the molecule. The Stark shift [Eq. (14)] can evolve through several means: fluctuations in the field magnitude E, changes in the orientation of the electric field, and changes in the orientation of the difference dipole vector. The last of these, rotation of the difference dipole due to physical rotation of the molecule, is the source of RISD or RISS, while the first two are the sources of structural spectral diffusion (SSD) or SSS.

To evaluate the FFCFs with weighting by input and output polarizations, we must introduce several additional quantities. In general, for fluorescent molecules, the absorption transition dipole moment $\hat{\mu}_{\mathrm{A}}$ and emission transition dipole moment $\hat{\mu}_{\mathrm{E}}$ (unit vectors) are not coincident. For definitiveness, we take the absorption transition dipole moment to coincide with the symmetry axis of the probe molecule that we will track for rotational diffusion. There would be no difference if the emission dipole instead corresponded to the symmetry axis. The absorption dipole coordinate system in the lab frame is $\Omega_{\mathrm{LA}} = (\phi_{\mathrm{LA}}, \theta_{\mathrm{LA}}, \chi_{\mathrm{LA}})$. The total angle from the absorption dipole moment to the emission dipole moment is δ, and the angle from absorption dipole to the difference dipole is ψ. These three unit vectors are assumed rigidly attached to one another and their relations are displayed in Fig. 8. The absorption dipole moment $\hat{\mu}_{\mathrm{A}}$ is initially excited by interaction with the incoming laser field. Following this, the molecule can rotate, changing the orientation of both $\hat{\mu}_E$ and $\hat{\mu}_D$. This changes both the contribution of the molecule to emission in a particular observation polarization and the frequency through the Stark effect.

We have expressed the Stark shift [Eq. (14)] in terms of difference dipole coordinates in the field frame, but the averages over molecular orientations will be done in the lab frame. Additionally,

polarization-weighting (as necessary) must be done according to the absorption and emission transition dipoles in the lab frame, as the laser polarizations are fixed in the lab frame. We can now cast the Stark shift in its most useful form for changes in the coordinate system, noting that $\cos\theta = P_1(\cos\theta) = D^1_{00}(\Omega)$, where $\Omega = (\phi, \theta, \chi)$ is a general Euler angle, P_l is the Legendre polynomial of order l, and D^l_{mn} are the Wigner D-matrices or rotation matrices.[58,59] Then, we have

$$\Delta\omega = -\Delta\mu E \times D^1_{00}(\Omega_{\mathrm{FD}}). \tag{15}$$

The rotation matrices are simply related to the spherical harmonics when one of m, n is zero: $Y^m_l(\theta,\phi) = \sqrt{(2l+1)/4\pi}D^l_{m0}{}^*(\phi,\theta,\chi)$. Hence, there is a straightforward representation under rotation or change in the coordinate system[41,58–60]

$$D^l_{m0}(\Omega_{\mathrm{FD}}) = \sum_{m=-l}^{l} D^l_{mn}(\Omega_{\mathrm{FL}}) D^l_{n0}(\Omega_{\mathrm{LD}}). \tag{16}$$

Applying Eq. (16) twice to Eq. (15) to introduce the lab frame (L) as well as the absorption frame (A), we obtain

$$\Delta\omega = -\Delta\mu E \sum_{m,n} D^1_{0m}(\Omega_{\mathrm{FL}}) D^1_{mn}(\Omega_{\mathrm{LA}}) D^1_{n0}(\Omega_{\mathrm{AD}}) \tag{17}$$

in which the electric field and absorption transition dipole are clearly related to the lab frame. The transformation from the A to D frame is defined as $\Omega_{\mathrm{AD}} = (\phi_{\mathrm{AD}}, \psi, \chi_{\mathrm{AD}})$.

For calculation of the observables, one final assumption is needed: the orientational dynamics of the probe molecule and the dynamics of the electric field created by the surroundings (both in orientation and magnitude) are statistically independent.[29] While there may be a potential energy minimum for interaction of the probe with the field, other constraints of the liquid or solid medium force the molecule to adopt all possible orientations relative to the field with equal probability. This approximation has been found to break down in certain situations recently, when the field interacts very strongly with the molecular dipole moment.[36] However, we shall treat only the weaker interacting cases for which the sole consequence of the field is a frequency shift through the Stark effect.

From the above, we immediately can conclude that $\langle\Delta\omega\rangle = 0$ because $\langle D^l_{mn}(\Omega)\rangle = 0$ for $l > 0$.[58,59] Then, $\langle\omega\rangle = \omega_0$ and the instantaneous frequency fluctuation is

$$\begin{aligned}\delta\omega(t) &\equiv \omega(t) - \langle\omega\rangle = \Delta\omega(t) \\ &= -\Delta\mu E(t) \sum_{m,n} D^1_{0m}(\Omega_{\mathrm{FL}}(t)) D^1_{mn}(\Omega_{\mathrm{LA}}(t)) D^1_{n0}(\Omega_{\mathrm{AD}}),\end{aligned} \tag{18}$$

where the explicit time dependence of fluctuating quantities appearing in Eq. (17) has been included in Eq. (18).

We denote a polarization-weighted average by $\langle\cdots\rangle_p$, where $p = \langle EEAA\rangle$ is the polarization configuration, with EE and AA each denoting a pair of transition dipole–laser field interactions. AA is the absorption polarization and EE is the emission polarization. The explicit form of the polarization-weighted average will be given below. The weighting is in terms of Ω_{LA} coordinates, so factors that do not depend on the absorption dipole orientation reduce to regular averages $\langle\cdots\rangle$.

Now, we construct the polarization-weighted FFCF (PW-FFCF) using Eq. (18),

$$\begin{aligned}C_p(t) &\equiv \langle\delta\omega(t)\delta\omega(0)\rangle_p \\ &= \Delta\mu^2 \sum_{m,n,m',n'} \left\langle E(t)E(0) D^1_{0m}(\Omega_{\mathrm{FL}}(t)) D^1_{0m'}(\Omega_{\mathrm{FL}}(0)) D^1_{mn}(\Omega_{\mathrm{LA}}(t)) D^1_{m'n'}(\Omega_{\mathrm{LA}}(0)) D^1_{n0}(\Omega_{\mathrm{AD}}) D^1_{n'0}(\Omega_{\mathrm{AD}})\right\rangle_p \\ &= \Delta\mu^2 \sum_{m,n,m',n'} D^1_{n0}(\Omega_{\mathrm{AD}}) D^1_{n'0}(\Omega_{\mathrm{AD}}) \left\langle E(t)E(0) D^1_{0m}(\Omega_{\mathrm{FL}}(t)) D^1_{0m'}(\Omega_{\mathrm{FL}}(0))\right\rangle \left\langle D^1_{mn}(\Omega_{\mathrm{LA}}(t)) D^1_{m'n'}(\Omega_{\mathrm{LA}}(0))\right\rangle_p \\ &= \Delta\mu^2 \sum_{m,n} D^1_{n0}(\Omega_{\mathrm{AD}}) D^1_{-n0}(\Omega_{\mathrm{AD}}) \left\langle E(t)E(0) D^1_{0m}(\Omega_{\mathrm{FL}}(t)) D^1_{0,-m}(\Omega_{\mathrm{FL}}(0))\right\rangle \left\langle D^1_{mn}(\Omega_{\mathrm{LA}}(t)) D^1_{-m,-n}(\Omega_{\mathrm{LA}}(0))\right\rangle_p \\ &= \Delta\mu^2 \sum_{m,n} \left|D^1_{n0}(\Omega_{\mathrm{AD}})\right|^2 \left\langle E(t)E(0) D^1_{0m}(\Omega_{\mathrm{FL}}(t)) D^1_{0m}{}^*(\Omega_{\mathrm{FL}}(0))\right\rangle \left\langle D^1_{mn}(\Omega_{\mathrm{LA}}(t)) D^1_{mn}{}^*(\Omega_{\mathrm{LA}}(0))\right\rangle_p \\ &= \Delta\mu^2 \left\langle E(t)E(0) D^1_{0m}(\Omega_{\mathrm{FL}}(t)) D^1_{0m}{}^*(\Omega_{\mathrm{FL}}(0))\right\rangle \sum_{m,n} d^1_{n0}(\psi)^2 \left\langle D^1_{mn}(\Omega_{\mathrm{LA}}(t)) D^1_{mn}{}^*(\Omega_{\mathrm{LA}}(0))\right\rangle_p.\end{aligned} \tag{19}$$

Several simplifications were made between the second and final lines of Eq. (19). For the third line, we separated the correlation functions of independent parameters, i.e., the electric field fluctuations and molecular orientational fluctuations. Note that only the correlation function involving absorption dipole rotation (LA coordinates) has a polarization weight p-dependence. For the fourth line, we first use the identity derived previously[29] for correlation functions of magnitude and direction fluctuations that are not statistically independent

$$\left\langle E(t)E(0) D^l_{rs}(\Omega(t)) D^{l'}_{r's'}(\Omega(0))\right\rangle \propto \delta_{r,-r'}\delta_{s,-s'}, \tag{20}$$

followed by a general orthogonality condition of correlation functions over two D-matrices for rotational diffusion,

$$\left\langle D^l_{mn}(\Omega_{\mathrm{LA}}(t)) D^{l'}_{-mn'}(\Omega_{\mathrm{LA}}(0))\right\rangle_p \propto \delta_{n,-n'}. \tag{21}$$

The orthogonality condition [Eq. (21)] follows directly from the form of the probability evolution Green's function (see Sec. IV B) and holds independently of polarization condition. For the fifth line of Eq. (19), we use the following identity: $D^{l}_{m,n}{}^{*}(\Omega) = (-1)^{m-n} D^{l}_{-m,-n}(\Omega)$. In the sixth line, we refer to the explicit form of the D-matrices, $D^{l}_{mn}(\phi,\theta,\chi) = \exp(-i\phi) d^{l}_{mn}(\theta) \exp(-i\chi)$, where d^{l}_{mn} is Wigner's small d-matrix, a real valued function.[58,59] Finally, in the sixth line, we also factored out the correlation function of field magnitude and direction from the sum, as it is an isotropic property and thus does not depend on the index m. This fact is analogous to the energy (a scalar) of an atomic p state (orbital angular momentum $l = 1$) in the absence of external fields: the magnetic quantum number m_l makes no difference.

Just as in the previous case for 2D IR FFCFs with polarization dependence, we find the PW-FFCF for an electronic transition factors into two terms

$$C_p(t) = S(t) R_p(t), \tag{22}$$

with a polarization-independent SSD or SSS term,

$$S(t) = \Delta\mu^2 \left\langle E(t)E(0) D^{1}_{0m}(\Omega_{\mathrm{FL}}(t)) D^{1}_{0m}{}^{*}(\Omega_{\mathrm{FL}}(0)) \right\rangle, \tag{23}$$

and a polarization configuration p-dependent RISD or RISS term,

$$R_p(t) = \sum_{m,n} d^{1}_{n0}(\psi)^2 \left\langle D^{1}_{mn}(\Omega_{\mathrm{LA}}(t)) D^{1}_{mn}{}^{*}(\Omega_{\mathrm{LA}}(0)) \right\rangle_p. \tag{24}$$

The SSD factor [Eq. (23)] has identical meaning to previous results for the first order Stark effect,[29] though its apparent form can change depending on the definition of the angles appearing and the use of identities for D-matrices to move the m index between the first and the second position. Using the addition theorem for spherical harmonics,[58,59] both Eq. (23) and previously published expressions for the SSD[29] become

$$\begin{aligned} S(t) &= \frac{\Delta\mu^2}{3} \left\langle E(t)E(0) P_1\big(\cos(\Theta_{\mathrm{F}}(t))\big) \right\rangle \\ &= \frac{\Delta\mu^2}{3} \left\langle E(t)E(0) \cos\big(\Theta_{\mathrm{F}}(t)\big) \right\rangle \\ &= \frac{\Delta\mu^2}{3} \left\langle \vec{E}(t) \cdot \vec{E}(0) \right\rangle, \end{aligned}$$

with $\Theta_{\mathrm{F}}(t)$ being the angle between the field frame Z_{F} axis at time t and $t = 0$. The initial value of Eq. (24), and therefore Eq. (23) [below we find Eq. (25) is normalized to unity], is $S(0) = \Delta\mu^2 \langle E^2 \rangle / 3$. This initial value is also equal to Δ^2 of Eq. (A8) (see the Appendix) and thus determines the reorganization energy λ.

The polarization-dependent RISS term is not in the same form as the 2D IR results derived previously;[28,29] there is an explicit dependence on the angle ψ between the absorption dipole and difference dipole. The polarization weighting is also not the same as in the previous treatment because the absorption and emission dipoles do not have to coincide, their angle being δ (Fig. 8). In Sec. IV B, we evaluate Eq. (25) for $R_p(t)$ to describe RISS (or RISS).

B. Evaluation of the polarization-dependent RISD factors for electronic transitions

To evaluate the RISS factor in Eq. (25), we must perform a correlation function average with polarization weighting. For quantities depending on the orientational coordinates Ω_t and Ω_0 of the molecular frame in the lab frame, separated by a time t, the polarization-weighted correlation function is defined as[28]

$$\begin{aligned} \langle \cdots \rangle_{p=EEAA} = \frac{1}{I_{EEAA}(t)} \int \mathrm{d}\Omega_t \int \mathrm{d}\Omega_0 (\cdots) (\hat{\varepsilon}_E \cdot \hat{\mu}(\Omega_{\mathrm{LE},t}))^2 \\ \times G(t;\Omega_t,\Omega_0) (\hat{\varepsilon}_A \cdot \hat{\mu}(\Omega_0))^2 P(\Omega_0), \end{aligned} \tag{25}$$

where the normalization factor is given by[28,54,61]

$$\begin{aligned} I_{EEAA}(t) = \int \mathrm{d}\Omega_t \int \mathrm{d}\Omega_0 (\hat{\varepsilon}_E \cdot \hat{\mu}(\Omega_{\mathrm{LE},t}))^2 \\ \times G(t;\Omega_t,\Omega_0) (\hat{\varepsilon}_A \cdot \hat{\mu}(\Omega_0))^2 P(\Omega_0). \end{aligned} \tag{26}$$

Here, $G(t;\Omega_t,\Omega_0)$ is the probability evolution Green's function for orientational relaxation, $P(\Omega_0) = 1/(8\pi^2)$ is the equilibrium distribution of initial orientational coordinates, $\Omega_{\mathrm{LE},t}$ is the emission dipole orientation given an absorption dipole orientation Ω_t, and $(\hat{\varepsilon} \cdot \hat{\mu}(\Omega))^2$ are the overlap factors between laser field polarizations $\hat{\varepsilon}$ and transition dipole orientations $\hat{\mu}$, resulting in polarization weighting. Note that we are writing integration over a volume element $\mathrm{d}\Omega$ as an abbreviation for integration over all three Euler angles

$$\int \mathrm{d}\Omega \equiv \int_0^{\pi} \sin\theta \mathrm{d}\theta \int_0^{2\pi} \mathrm{d}\phi \int_0^{2\pi} \mathrm{d}\chi.$$

The normalization factor (26) is the familiar function for decay of fluorescence intensity or pump-probe signal in polarization-selective measurements.[54,61] This normalization is necessary because the polarization weight factors in Eq. (25) cause a varying number of molecules to contribute to the signal as a function of time and polarization configuration.

An important consideration before we can evaluate Eq. (24) using Eq. (25) is the fact that Ω_t and Ω_0 are taken to be the coordinates of the *absorption* transition dipole in G, but one of the weight factors is in terms of the *emission* transition dipole coordinates. For an arbitrary dipole expressed in the lab frame coordinates, the interaction factors are given in Table IV. We will evaluate polarization configurations where the emission polarization is fixed along the lab Z-axis. It is straightforward to rewrite the Z-polarized emission interaction factor in terms of the absorption dipole orientation $\Omega_t = \Omega_{\mathrm{LA}}(t)$ and the transformation from the absorption to emission frame $\Omega_{\mathrm{AE}} = (\phi_{\mathrm{AE}}, \delta, \chi_{\mathrm{AE}})$ using Table IV and Eq. (16),

$$\begin{aligned} (\hat{\varepsilon}_Z \cdot \hat{\mu}(\Omega_{\mathrm{LE}}))^2 &= \frac{1}{3} + \frac{2}{3} D^{2}_{00}(\Omega_{\mathrm{LE}}) \\ &= \frac{1}{3} + \frac{2}{3} \sum_m D^{2}_{0m}(\Omega_{\mathrm{LA}}) D^{2}_{m0}(\Omega_{\mathrm{AE}}). \end{aligned} \tag{27}$$

The final quantity needed for evaluation of our results is the probability evolution Green's function, which for a symmetric rotor undergoing rotational randomization takes the following form:[61,62]

$$G(t;\Omega_t,\Omega_0) = \sum_{l=0}^{\infty} \sum_{m=-l}^{l} \sum_{n=-l}^{l} \frac{2l+1}{8\pi^2} C_l(t) D^{l}_{mn}(\Omega_t) D^{l}_{mn}{}^{*}(\Omega_0). \tag{28}$$

TABLE IV. Laser field interaction weights in the laboratory frame with the Wigner D-matrix representation. Laser field polarizations in the lab frame are given by the unit vectors $\hat{\varepsilon}$. Here, MA refers to a polarization at the magic angle measured from the *Z*-axis toward the *X*-axis, and $\Omega = (\phi, \theta, \chi)$ denotes the Euler angles of the dipole $\hat{\mu}$ in the lab frame.

Interaction	Coordinate representation	*D*-matrix representation
$(\hat{\varepsilon}_Z \cdot \hat{\mu}(\Omega))^2$	$\cos^2\theta$	$\frac{1}{3} + \frac{2}{3}D^2_{00}(\Omega)$
$(\hat{\varepsilon}_X \cdot \hat{\mu}(\Omega))^2$	$\sin^2\theta\cos^2\phi$	$\frac{1}{3} - \frac{1}{3}D^2_{00}(\Omega) + \frac{1}{\sqrt{6}}\left(D^2_{20}(\Omega) + D^2_{-20}(\Omega)\right)$
$(\hat{\varepsilon}_Y \cdot \hat{\mu}(\Omega))^2$	$\sin^2\theta\sin^2\phi$	$\frac{1}{3} - \frac{1}{3}D^2_{00}(\Omega) - \frac{1}{\sqrt{6}}\left(D^2_{20}(\Omega) + D^2_{-20}(\Omega)\right)$
$(\hat{\varepsilon}_{MA} \cdot \hat{\mu}(\Omega))^2$	$\frac{1}{3}\cos^2\theta + \frac{2}{3}\sin^2\theta\cos^2\phi$	$\frac{1}{3} + \frac{2}{3\sqrt{6}}\left(D^2_{20}(\Omega) + D^2_{-20}(\Omega)\right)$

Here, $C_l(t) = \langle P_l(\hat{\mu}_A(t) \cdot \hat{\mu}_A(0))\rangle$ is the orientational correlation function of order l for the absorption transition dipole moment unit vector. In the simple case of orientational free diffusion, with diffusion constant D_R, the orientational correlation function is $C_l(t) = \exp(-l(l+1)D_R t)$. More complex forms of the orientational correlation function appear when there are periods of restricted orientational diffusion (wobbling-in-a-cone);[41] details of such wobbling motions were discussed in Sec. III 3.

With all quantities appearing in Eqs. (26)–(28) expressed in terms of the Wigner D-matrices, we can use analytical results for integrals over 2 and 3 *D*-matrices having the same coordinates,[58,59]

$$\int d\Omega D^l_{mn}(\Omega) D^{l'}_{m'n'}{}^*(\Omega) = \frac{8\pi^2}{2l+1}\delta_{l,l'}\delta_{m,m'},\delta_{n,n'} \tag{29}$$

and

$$\int d\Omega D^{l_1}_{m_1n_1}(\Omega) D^{l_2}_{m_2n_2}(\Omega) D^{l_3}_{m_3n_3}(\Omega) = 8\pi^2 \begin{pmatrix} l_1 & l_2 & l_3 \\ m_1 & m_2 & m_3 \end{pmatrix}\begin{pmatrix} l_1 & l_2 & l_3 \\ n_1 & n_2 & n_3 \end{pmatrix}, \tag{30}$$

where the brackets in Eq. (30) are Wigner's 3-J symbols, whose values are tabulated[58,59] or easily generated by various computer packages. Immediately, we can reduce the sum over all l using Eq. (28) in Eq. (25) to a small, finite set. We find products of rotation matrices with total angular momenta l, 1, and 0; or l, 1, and 2. The 3-J symbol will be nonzero only if the triangle condition is satisfied,[58,59] meaning l can take on the values of 1, 2, or 3 only. Further simplification of terms that appear in the expansion is possible using the requirements that $m_1 + m_2 + m_3 = 0$ and $n_1 + n_2 + n_3 = 0$ for nonzero 3-J symbols.

Evaluating all integrals in Eq. (24) with Eq. (25) and in Eq. (26) using the above identities and simplifications, with assistance from Mathematica[63] in summing the terms that survive, analytical results in closed form are obtained. For the normalization factors, we recover well known expressions for polarization-selective signal amplitude in third order spectroscopic measurements,[54,61]

$$I_{ZZZZ}(t) = (1 + (4/5)P_2(\cos\delta)C_2(t))/9, \tag{31a}$$

$$I_{ZZXX}(t) = (1 - (2/5)P_2(\cos\delta)C_2(t))/9, \tag{31b}$$

and

$$I_{iso}(t) = 1/9. \tag{31c}$$

Equations (31a) and (31b) give the familiar expression for the fluorescence (or pump probe) anisotropy with $\delta = 0$,[61]

$$r(t) = \frac{I_{ZZZZ}(t) - I_{ZZXX}(t)}{I_{ZZZZ}(t) + 2I_{ZZXX}(t)} = \frac{2}{5}P_2(\cos\delta)C_2(t).$$

The polarization-dependent RISS or RISD factors, $R_p(t)$, appear in their most general form as follows:

$$R_{ZZZZ}(t) = \frac{1}{75(1 + (4/5)P_2(\cos\delta)C_2(t))} \times \begin{bmatrix} C_1(t)[75 + 12P_2(\cos\delta)(1 + P_2(\cos\psi))] \\ +C_2(t)[20P_2(\cos\delta)(1 - P_2(\cos\psi))] \\ +C_3(t)[4P_2(\cos\delta)(7 + 2P_2(\cos\psi))] \end{bmatrix}, \tag{32a}$$

$$R_{ZZXX}(t) = \frac{1}{75(1 - (2/5)P_2(\cos\delta)C_2(t))} \times \begin{bmatrix} C_1(t)[75 - 6P_2(\cos\delta)(1 + P_2(\cos\psi))] \\ -C_2(t)[10P_2(\cos\delta)(1 - P_2(\cos\psi))] \\ -C_3(t)[2P_2(\cos\delta)(7 + 2P_2(\cos\psi))] \end{bmatrix}, \tag{32b}$$

and

$$R_{iso}(t) = C_1(t). \tag{32c}$$

These are called $S_\parallel(t)$, $S_\perp(t)$, and $S_{iso}(t)$ in Eqs. (6)–(8), respectively.

It is straightforward to check that at $t = 0$, assuming $C_1(0) = C_2(0) = C_3(0) = 1$ for complete orientational correlation, $R_p(0) = 1$ for all three configurations shown in Eq. (32). Thus, the RISS factor of Eq. (24) is normalized to unity. The same result for the isotropic (iso) average, done either without polarization weight or with a magic angle (MA) weighted average (Table IV) is obtained in Eqs. (31c) and (32c).

Several special cases for the angles δ and ψ are considered. Suppose δ is at the magic angle $\delta_{MA} = \cos^{-1}\left(1/\sqrt{3}\right)$, which is defined by $P_2(\cos\delta_{MA}) = 0$. Then, we find

$$R_{ZZZZ}(t) = R_{ZZXX}(t) = R_{iso}(t) = C_1(t). \tag{33}$$

That is to say, when the absorption and emission dipoles are at the magic angle to one another, we no longer see a dependence of the FFCF on polarization. The RISS contribution is $C_1(t)$ in all cases. RISS contributes equally to the observed decays in all polarization configurations.

For most vibrational transitions and likely many electronic transitions to a first excited state, the absorption and emission dipole moments coincide, i.e., $\delta = 0$ and thus, $P_2(\cos\delta) = 1$. In this case, Eqs. (32a) and (32b) become simpler and have the form

$$R_{ZZZZ}(t) = \frac{1}{75(1+(4/5)C_2(t))}\begin{bmatrix} C_1(t)[3(29+4P_2(\cos\psi)] \\ +C_2(t)[20(1-P_2(\cos\psi))] \\ +C_3(t)[4(7+2P_2(\cos\psi))] \end{bmatrix}, \tag{34a}$$

$$R_{ZZXX}(t) = \frac{1}{75(1-(2/5)C_2(t))}\begin{bmatrix} C_1(t)[3(23-2P_2(\cos\psi))] \\ -C_2(t)[10(1-P_2(\cos\psi))] \\ -C_3(t)[2(7+2P_2(\cos\psi))] \end{bmatrix}, \tag{34b}$$

with the isotropic result unchanged. If we make the final assumption that the difference dipole moment is also in the direction of the absorption and emission dipole moments ($\psi = 0$), then Eq. (34) reduces to the normalized RISD factors published previously that were used for vibrational transitions,[28,29]

$$R_{ZZZZ}(t) = \frac{3}{25}\left[\frac{11C_1(t)+4C_3(t)}{1+(4/5)C_2(t)}\right], \tag{35a}$$

$$R_{ZZXX}(t) = \frac{3}{25}\left[\frac{7C_1(t)-2C_3(t)}{1-(2/5)C_2(t)}\right]. \tag{35b}$$

Note that $P_2(\cos\psi) = 1$, when applied to either Eq. (32) or (34) eliminates the $C_2(t)$ contribution to the numerator but not the denominator. No matter what values δ and ψ take, the isotropic (magic angle) polarization configuration gives the same, isotropically averaged result $C_1(t)$.

The RISS or RISD results for three polarization configurations: $\langle ZZZZ\rangle$ (parallel), $\langle ZZYY\rangle$ (perpendicular), and isotropic (magic angle) were calculated above. Only two of these are actually independent, allowing us to calculate the expressions for any angle between the absorption and emission polarization.[28] We take the parallel and perpendicular results [Eqs. (34a) and (34b)] to be our fundamental pair. Suppose we always detect emission polarized along Z, but with excitation at an arbitrary angle α from Z toward X. The absorption weight factor takes the following form:

$$(\hat{\varepsilon}_\alpha \cdot \hat{\mu}(\Omega))^2 = \cos^2\alpha(\hat{\varepsilon}_Z \cdot \hat{\mu}(\Omega))^2 + \sin^2\alpha(\hat{\varepsilon}_X \cdot \hat{\mu}(\Omega))^2. \tag{36}$$

Therefore, by simple inspection of Eqs. (25) and (26), we can write the polarization-dependent RISD factor [Eq. (24)] as

$$R_{ZZ\alpha\alpha}(t) = \frac{\cos^2\alpha I_{ZZZZ}(t)R_{ZZZZ}(t) + \sin^2\alpha I_{ZZXX}(t)R_{ZZXX}(t)}{\cos^2\alpha I_{ZZZZ}(t) + \sin^2\alpha I_{ZZXX}(t)}. \tag{37}$$

Using Eq. (37), and setting α to the magic angle, we have $\cos^2\alpha = 1/3$ and $\sin^2\alpha = 2/3$, and thus, we can immediately verify that the isotropic result [Eq. (32c)] follows from Eqs. (32a) and (32b).[28]

We conclude this section with some comments on the use of Eqs. (32) [which become Eqs. (6)–(8) upon multiplication by the SSS factor]. The angles δ and ψ are constants of the electronic or vibrational transition of a given molecule and can, in principle, be determined by other spectroscopic methods[55] or with electronic structure calculations.[1] The correlation function $C_2(t)$ can be measured directly for the transition of interest using, e.g., the pump-probe or fluorescence anisotropy.[29,54,61] With an appropriate model for the orientational dynamics (e.g., free diffusion, jump diffusion, or wobbling-in-a-cone), measurement of the second order orientational correlation function allows $C_1(t)$ and $C_3(t)$ to be constructed from the parameters describing $C_2(t)$.[29] Thus, the RISS or RISD factors [Eqs. (25) and (26)] have no adjustable parameters, leaving the only unknown quantity the SSS or SSD factor [see Eq. (6)–(8)]. Thus, by knowing the time dependent anisotropy of a probe in its environment, one can separate the effects of RISS from the material's structural relaxation for any polarization. By measuring multiple polarizations and fitting the data globally, the separation can be achieved with greater confidence.

V. CONCLUDING REMARKS

In a wide range of prior studies,[1–6,8,10,13,37,64–66] a single polarization has been sufficient to measure the dynamic Stokes shift of a fluorescence probe. These dynamic Stokes shift measurements report on the solvation dynamics of the medium, which is usually a small molecule liquid. We refer to this as the structural Stokes shift (SSS). Here, we have observed a significant polarization-dependence in dynamic Stokes shift measurements on the chromophore C153 in the polymer PMMA [see Fig. 3(a)]. In systems where chromophore reorientation occurs on time scales comparable to structural dynamics of the medium, the probe reorientation contributes to the observed Stokes shift measurements in addition to the SSS. When the Stokes shift chromophore is electrically excited, there is a large change in its dipole direction and/or magnitude. The coupling to the medium is through this change in dipole. Therefore, the coupling is inherently vectorial in nature, e.g., a first order Stark effect. Reorientation of the chromophore changes its dipole direction, changing the coupling. The result is that the reorientation of the chromophore contributes to the Stokes shift. This effect is referred to as reorientation induced Stokes shift (RISS). Therefore, the Stokes shift has both SSS and RISS components. The manifestation of RISS depends on the fluorescence observation polarization relative to the excitation polarization, giving rise to the polarization dependence seen in Fig. 3(a).

A detailed theory was developed for the RISS effect. This theory is an extension of the theory that describes reorientational induced spectral diffusion (RISD) that has been observed in 2D IR experiments.[28–36] The theory shows the relationship between the chromophore's orientational relaxation and the polarization-dependence of the fluorescence [see Eqs. (6)–(8)]. One of the important results of the theory is that the total time dependent Stokes shift is the product of the SSS and RISS contributions [Eq. (22)]. The time-dependent contributions to the RISS can be obtained by independent measurements of the orientational relaxation of the chromophore using fluorescence anisotropy measurements. In addition, it is necessary to know the angle between the absorption transition dipole direction and the dipole difference vector that result from the creation of the new dipole in the excited state and the angle between the absorption and emission transition dipole directions. In principle, these angles can be measured by independent experiments. For the C153/PMMA system, both of these angles are zero, and all of the information necessary to determine the RISS time-dependent contribution to the

Stokes shift was determined from the fluorescence anisotropy measurements. With the RISS term known, the desired SSS dynamics were determined. Fits to the polarization-dependent data are shown in Fig. 7(a). The fast structural dynamic time constants are given in Table III.

Dynamic Stokes shifts measurements and 2D IR show the manifestation of probe rotation in their polarization-dependent observables. Both experiments are directly related to the frequency-frequency correlation function (FFCF) of the transition under observation. In addition to the theoretical development of the RISS effect given in Sec. IV, the detailed relationship between the dynamic Stokes shift and the FFCF is derived in the Appendix. Other experiments with observables that are theoretically related to the FFCF, such as hole burning, homodyne echoes, or transient absorption, should also display the equivalent of RISS and RISD.

In complex chemical systems such as polymers, the probe orientational relaxation and the fast structural relaxations (tens of picoseconds to tens of nanoseconds) may frequently occur on the same time scales. To obtain the SSS, it is necessary to remove the RISS contribution as was done in this first study of the effect and of fast polymer dynamics. The results presented here open a path for dynamic Stokes shift measurement to be used for detailed studies of polymers and other systems in which the structural and probe reorientational dynamics are on the same time scales.

ACKNOWLEDGMENTS

This work was supported by the Office of Naval Research by ONR: N00014-17-1-2656 (D.J.H., S.M.F.-C., and M.D.F.). Additional support was provided by Division of Chemical Sciences, Geosciences, and Biosciences, Office of Basic Energy Sciences of the U.S. Department of Energy through Grant No. DE-FG03-84ER13251 (J.E.T., P.L.K., and M.D.F.). Polarized steady state fluorescent spectra were collected at the Stanford Nano Shared Facilities (SNSF), supported by the National Science Foundation under award ECCS-1542152. J.E.T. thanks the NSF for a graduate fellowship, and P.L.K. acknowledges an ARCS fellowship for partial financial support. J.E.T. also thanks Atsunori Sakurai, Heather Bailey, and Steven Yamada for useful discussions.

APPENDIX: THE STOKES SHIFT CORRELATION FUNCTION

The evolution of the frequency maximum of fluorescence emission, the dynamic Stokes shift, tracks the fluctuations of the probe and solvent interactions to accommodate the excited-state fluorophore's change in the dipole direction and/or magnitude. Denoting the maximum frequency of emission at a time t by $\omega_0(t)$, we can express the progress of the Stokes shift through the Stokes shift correlation function (SSCF),[1,67,68]

$$S(t) = \frac{\omega_0(t) - \omega_0(\infty)}{\omega_0(0) - \omega_0(\infty)}. \tag{A1}$$

In accordance with linear response theory,[15] $N(t)$ has been interpreted as the correlation function of the equilibrium fluctuations in solvation energy, E, or $N(t) = \langle \delta E(t)\delta E(0)\rangle / \langle \delta E^2 \rangle$.[68] Fluctuations in solvation energy are also identified with fluctuations of the instantaneous absorption frequency for an electronic (or vibrational) transition, the source of spectral diffusion.[25] In this section, we make quantitative the relationship between spectral diffusion of the electronic absorption frequency and dynamic Stokes shift of the fluorescence emission frequency, demonstrating that the same correlation function describes both.

Time-resolved fluorescence spectroscopy can be described, like many other techniques including two-dimensional (2D) optical spectroscopy[52] and pump-probe spectroscopy, using third-order nonlinear response functions from diagrammatic perturbation theory.[25] Within this framework, we view the fluorescence process as follows. A single interaction between the probe and the laser electric field occurs at time zero, followed immediately by the resulting coherence experiencing a field interaction due to a virtual photon to populate the excited state. The probe molecule experiences dynamics in the excited state until the field of another virtual photon returns the system to a coherence state, after which the fluorescence electric field is emitted. Thus, the time intervals that enter the third order response function are as follows: $t_1 = 0$ is the first coherence time following the initial electric field interaction, t_2 is the waiting period in the population (excited) state, and t_3 is the final coherence time over which the fluorescence is emitted. As the emission is typically frequency-resolved, the experimental observable follows from an experimental Fourier transform over t_3 performed by a spectrograph.

Under the extremely useful Condon approximation and truncation of the cumulant expansion to second order, the linear and nonlinear response functions are completely determined by a single (generally complex) quantity, the line shape function,

$$g(t) = \int_0^t \mathrm{d}\tau_2 \int_0^{\tau_2} \mathrm{d}\tau_1 C(\tau_1), \tag{A2}$$

with the two-time energy gap correlation function $C(t) = C'(t) + iC''(t)$. Here, $C'(t)$ is real and even, while $C''(t)$ is real and odd.[25] $C(t)$, a quantum mechanical correlation function of the energy operator (in units of angular frequency), is the fundamental quantity connecting microscopic dynamics with the linear and nonlinear spectroscopic observables.[25] In the semiclassical limit, the real part of $C(t)$ is the correlation function of electronic (or vibrational) absorption frequency fluctuations $\delta\omega(t) = \omega(t) - \langle\omega\rangle$, that is,

$$C'(t) = \langle \delta\omega(t)\delta\omega(0)\rangle. \tag{A3}$$

This connection is frequently of great value in 2D IR spectroscopy, allowing extraction of the frequency-frequency correlation function (FFCF) $C'(t)$ from the waiting-time-dependent 2D line shape.[23,53] Thus, the real part of $g(t)$ is determined by the FFCF.

In the regime of linear response, where perturbations do not take the system far from equilibrium, the real and imaginary parts of $C(t)$ are not independent, being connected by the fluctuation-dissipation theorem.[25,69] Following Mukamel,[25] we define

$$M'(t) \equiv C'(t)/C'(0) \tag{A4}$$

as the normalized FFCF, with $\Delta^2 = C'(0) = \langle \delta\omega^2 \rangle$ being the mean square frequency fluctuation, and

$$\int_0^t \mathrm{d}\tau C''(\tau) \equiv \lambda\left[1 - M''(t)\right], \tag{A5}$$

with λ being the "reorganization energy." Then, the line shape function is Eq. (8.26) of Ref. 25,

$$g(t) = \Delta^2 \int_0^t d\tau_2 \int_0^{\tau_2} d\tau_1 M'(\tau_1) - i\lambda \int_0^t d\tau \left[1 - M''(\tau)\right]. \quad \text{(A6)}$$

Making use of the fluctuation dissipation theorem and in the high temperature limit, Mukamel gave the key results[25]

$$M'(t) = M''(t) \equiv M(t) \quad \text{(A7)}$$

and

$$\Delta^2 = \frac{2\lambda k_B T}{\hbar}, \quad \text{(A8)}$$

where T is the absolute temperature and k_B is Boltzmann's constant. That is to say, the real and imaginary parts of $g(t)$ in Eq. (A6) are determined by the *same* function $M(t)$, with the frequency fluctuation amplitude and reorganization energy linked by Eq. (A8). Thus, we can write [adapting Eq. (8.31) from Ref. 25]

$$\begin{aligned} g(t) &= \frac{2\lambda k_B T}{\hbar} \int_0^t d\tau_2 \int_0^{\tau_2} d\tau_1 M(\tau_1) - i\lambda \int_0^t d\tau [1 - M(\tau)] \\ &= \int_0^t d\tau_2 \int_0^{\tau_2} d\tau_1 C'(\tau_1) - i\lambda \int_0^t d\tau [1 - M(\tau)], \end{aligned} \quad \text{(A9)}$$

showing that the real part is given by $C'(t)$ (without normalization), while the imaginary part depends on the normalized $M(t) = C'(t)/C'(0)$ with $\lambda = \hbar C'(0)/(2k_B T)$ to set the scale.

In a fluorescence experiment, the line shape is determined by the nonlinear response functions $R_1^{(3)}$ and $R_2^{(3)}$ from Eq. (8.15) in Ref. 25. These are the nonrephasing and rephasing pathways, respectively, with the population period taking place in the excited state. The ground state response functions $R_3^{(3)}$ and $R_4^{(3)}$ naturally do not contribute to fluorescence and do not exhibit a Stokes shift. The relevant response function is thus

$$\begin{aligned} R_1^{(3)}(t_3, t_2, 0) &= R_2^{(3)}(t_3, t_2, 0) \\ &= \exp(-i\omega_{eg} t_3) \exp\big(-g^*(t_3) + g(t_2) \\ &\quad - g(t_2 + t_3) - g^*(t_2) + g^*(t_2 + t_3)\big) \\ &= \exp(-i\omega_{eg} t_3) \exp\big(-g^*(t_3) \\ &\quad + 2i\,\mathrm{Im}[g(t_2) - g(t_2 + t_3)]\big), \end{aligned} \quad \text{(A10)}$$

with ω_{eg} being the average electronic transition frequency for absorption. The time scale of solvation dynamics in t_2 is typically much longer than final coherence time t_3 for the field emission, so we make a short time approximation with t_3. Expanding $g(t_2 + t_3)$ around t_2 to first order in $t_2 + t_3$, using Eq. (A9), and taking the imaginary part, we find

$$\mathrm{Im}[g(t_2 + t_3)] \approx \mathrm{Im}[g(t_2)] - \lambda[1 - M(t_2)]t_3. \quad \text{(A11)}$$

Then, Eq. (A10) becomes

$$\begin{aligned} R_1^{(3)}(t_3, t_2, 0) &= \exp(-i\omega_{eg} t_3) \exp\big(-g^*(t_3) + 2i\lambda[1 - M(t_2)]t_3\big) \\ &= \exp\big(-i(\omega_{eg} - 2\lambda[1 - M(t_2)])t_3\big) \exp\big(-g^*(t_3)\big). \end{aligned} \quad \text{(A12)}$$

The first exponential clearly shows a shift in the oscillation frequency, depending on the population time t_2, of magnitude $-2\lambda[1 - M(t_2)]$. This is the Stokes shift. It decreases from zero at $t_2 = 0$ (no time for the probe and solute to rearrange to their new equilibrium) to a minimum of -2λ as $t_2 \to \infty$ (compare to Appendix 8B of Ref. 25 for the equivalent steady-state result). Ignoring any overall shift from the line shape factor $\exp(-g^*(t_3))$ in Eq. (A12), which would be independent of t_2, the emission frequency maximum is

$$\omega_0(t_2) = \omega_{eg} - 2\lambda[1 - M(t_2)]. \quad \text{(A13)}$$

Inserting Eq. (A13) into Eq. (A1), we find that the SSCF is given by $N(t) = M(t) = C'(t)/C'(0)$, the normalized FFCF.

REFERENCES

[1] M. Maroncelli and G. R. Fleming, "Picosecond solvation dynamics of coumarin 153: The importance of molecular aspects of solvation," J. Chem. Phys. **86**, 6221–6239 (1987).

[2] R. S. Moog, W. W. Davis, S. G. Ostrowski, and G. L. Wilson, "Solvent effects on electronic transitions in several coumarins," Chem. Phys. Lett. **299**, 265–271 (1999).

[3] F. Cichos, R. Brown, U. Rempel, and C. Von Borczyskowski, "Molecular dynamics simulations of the solvation of coumarin 153 in a mixture of an alkane and an alcohol," J. Phys. Chem. A **103**, 2506–2512 (1999).

[4] R. Karmakar and A. Samanta, "Solvation dynamics of coumarin-153 in a room-temperature ionic liquid," J. Phys. Chem. A **106**, 4447–4452 (2002).

[5] D. C. Khara and A. Samanta, "Fluorescence response of coumarin-153 in N-alkyl-N-methylmorpholinium ionic liquids: Are these media more structured than the imidazolium ionic liquids?," J. Phys. Chem. B **116**, 13430–13438 (2012).

[6] S. Arzhantsev, N. Ito, M. Heitz, and M. Maroncelli, "Solvation dynamics of coumarin 153 in several classes of ionic liquids: Cation dependence of the ultrafast component," Chem. Phys. Lett. **381**, 278–286 (2003).

[7] R. Karmakar and A. Samanta, "Dynamics of solvation of the fluorescent state of some electron donor–acceptor molecules in room temperature ionic liquids, [BMIM][$(CF_3SO_2)2N$] and [EMIM][$(CF_3SO_2)2N$]," J. Phys. Chem. A **107**, 7340–7346 (2003).

[8] J. E. Thomaz, H. E. Bailey, and M. D. Fayer, "The influence of mesoscopic confinement on the dynamics of imidazolium-based room temperature ionic liquids in polyether sulfone membranes," J. Chem. Phys. **147**, 194502 (2017).

[9] R. Richert, "Geometrical confinement and cooperativity in supercooled liquids studied by solvation dynamics," Phys. Rev. B **54**, 15762 (1996).

[10] D. Chakrabarty, D. Seth, A. Chakraborty, and N. Sarkar, "Dynamics of solvation and rotational relaxation of coumarin 153 in ionic liquid confined nanometer-sized microemulsions," J. Phys. Chem. B **109**, 5753–5758 (2005).

[11] R. Baumann, C. Ferrante, F. Deeg, and C. Bräuchle, "Solvation dynamics of nile blue in ethanol confined in porous sol–gel glasses," J. Chem. Phys. **114**, 5781–5791 (2001).

[12] D. Pant and N. E. Levinger, "Polar solvation dynamics of H_2O and D_2O at the surface of zirconia nanoparticles," J. Phys. Chem. B **103**, 7846–7852 (1999).

[13] H. N. Ghosh, J. B. Asbury, and T. Lian, "Direct observation of ultrafast electron injection from coumarin 343 to TiO_2 nanoparticles by femtosecond infrared spectroscopy," J. Phys. Chem. B **102**, 6482–6486 (1998).

[14] G. Ramakrishna, A. K. Singh, D. K. Palit, and H. N. Ghosh, "Effect of molecular structure on interfacial electron transfer dynamics of 7-N, N-dimethyl coumarin 4-acetic acid (DMACA) and 7-hydroxy coumarin 4-acetic acid (HCA) sensitized TiO_2 and ZrO_2 nanoparticles," J. Phys. Chem. B **108**, 12489–12496 (2004).

[15] L. Onsager, "Reciprocal relations in irreversible processes. II," Phys. Rev. **38**, 2265 (1931).

[16] M. Assael, K. Antoniadis, and J. Wu, "New measurements of the thermal conductivity of PMMA, BK7, and Pyrex 7740 up to 450 K," Int. J. Thermophys. **29**, 1257–1266 (2008).

[17]W. Goubau and R. Tait, "Short-time-scale measurement of the low-temperature specific heat of polymethyl methacrylate and fused silica," Phys. Rev. Lett. **34**, 1220 (1975).
[18]R. Bergman, F. Alvarez, A. Alegrıá, and J. Colmenero, "Dielectric relaxation in pmma revisited," J. Non-Cryst. Solids **235**, 580–583 (1998).
[19]M. Sharma, G. Madras, and S. Bose, "Cooperativity and structural relaxations in PVDF/PMMA blends in the presence of MWNTs: An assessment through SAXS and dielectric spectroscopy," Macromolecules **47**, 1392–1402 (2014).
[20]M. Cho, J.-Y. Yu, T. Joo, Y. Nagasawa, S. A. Passino, and G. R. Fleming, "The integrated photon echo and solvation dynamics," J. Phys. Chem. **100**, 11944–11953 (1996).
[21]B. L. Cotts, D. G. McCarthy, R. Noriega, S. B. Penwell, M. Delor, D. D. Devore, S. Mukhopadhyay, T. S. De Vries, and N. S. Ginsberg, "Tuning thermally activated delayed fluorescence emitter photophysics through solvation in the solid state," ACS Energy Lett. **2**, 1526 (2017).
[22]M. Delor, D. G. McCarthy, B. L. Cotts, T. D. Roberts, R. Noriega, D. D. Devore, S. Mukhopadhyay, T. S. De Vries, and N. S. Ginsberg, "Resolving and controlling photoinduced ultrafast solvation in the solid state," J. Phys. Chem. Lett. **8**, 4183–4190 (2017).
[23]K. Kwak, S. Park, I. J. Finkelstein, and M. D. Fayer, "Frequency-frequency correlation functions and apodization in two-dimensional infrared vibrational echo spectroscopy: A new approach," J. Chem. Phys. **127**, 124503 (2007).
[24]I. R. Piletic, K. J. Gaffney, and M. D. Fayer, "Structural dynamics of hydrogen bonded methanol oligomers: Vibrational transient hole burning studies of spectral diffusion," J. Chem. Phys. **119**, 423–434 (2003).
[25]S. Mukamel, *Principles of Nonlinear Optical Spectroscopy* (Oxford University Press, New York, 1995).
[26]J. A. Burt, X. Zhao, and J. L. McHale, "Inertial solvent dynamics and the analysis of spectral line shapes: Temperature-dependent absorption spectrum of β-carotene in nonpolar solvent," J. Chem. Phys. **120**, 4344–4354 (2004).
[27]D. B. Spry, A. Goun, and M. D. Fayer, "Identification and properties of the ^1L_a and ^1L_b states of pyranine (HPTS)," J. Chem. Phys. **125**, 144514 (2006).
[28]P. L. Kramer, J. Nishida, C. H. Giammanco, A. Tamimi, and M. D. Fayer, "Observation and theory of reorientation-induced spectral diffusion in polarization-selective 2D IR spectroscopy," J. Chem. Phys. **142**, 184505 (2015).
[29]P. L. Kramer, J. Nishida, and M. D. Fayer, "Separation of experimental 2D IR frequency-frequency correlation functions into structural and reorientation-induced contributions," J. Chem. Phys. **143**, 124505 (2015).
[30]J. Y. Shin, S. A. Yamada, and M. D. Fayer, "Dynamics of a room temperature ionic liquid in supported ionic liquid membranes vs the bulk liquid: 2D IR and polarized IR pump-probe experiments," J. Am. Chem. Soc. **139**, 311–323 (2016).
[31]J. Y. Shin, S. A. Yamada, and M. D. Fayer, "Carbon dioxide in a supported ionic liquid membrane: Structural and rotational dynamics measured with 2D IR and pump-probe experiments," J. Am. Chem. Soc. **139**, 11222–11232 (2017).
[32]A. Tamimi and M. D. Fayer, "Ionic liquid dynamics measured with 2D IR and IR pump-probe experiments on a linear anion and the influence of potassium cations," J. Phys. Chem. B **120**, 5842–5854 (2016).
[33]A. Tamimi, H. E. Bailey, and M. D. Fayer, "Alkyl chain length dependence of the dynamics and structure in the ionic regions of room-temperature ionic liquids," J. Phys. Chem. B **120**, 7488–7501 (2016).
[34]C. H. Giammanco, P. L. Kramer, S. A. Yamada, J. Nishida, A. Tamimi, and M. D. Fayer, "Carbon dioxide in an ionic liquid: Structural and rotational dynamics," J. Chem. Phys. **144**, 104506 (2016).
[35]C. H. Giammanco, P. L. Kramer, S. A. Yamada, J. Nishida, A. Tamimi, and M. D. Fayer, "Coupling of carbon dioxide stretch and bend vibrations reveals thermal population dynamics in an ionic liquid," J. Phys. Chem. B **120**, 549–556 (2016).
[36]Z. Ren and S. Garrett-Roe, "Reorientation-induced spectral diffusion of non-isotropic orientation distributions," J. Chem. Phys. **147**, 144504 (2017).
[37]N. Ito, S. Arzhantsev, M. Heitz, and M. Maroncelli, "Solvation dynamics and rotation of coumarin 153 in alkylphosphonium ionic liquids," J. Phys. Chem. B **108**, 5771–5777 (2004).
[38]N. Ito, S. Arzhantsev, and M. Maroncelli, "The probe dependence of solvation dynamics and rotation in the ionic liquid 1-butyl-3-methyl-imidazolium hexafluorophosphate," Chem. Phys. Lett. **396**, 83–91 (2004).
[39]J. A. Widegren, A. Laesecke, and J. W. Magee, "The effect of dissolved water on the viscosities of hydrophobic room-temperature ionic liquids," Chem. Commun. **0**, 1610–1612 (2005).
[40]P. Wirth, S. Schneider, and F. Dörr, "S_1-Lifetimes of triphenylmethane and indigo dyes determined by the two-photon-fluorescence technique," Opt. Commun. **20**, 155–158 (1977).
[41]G. Lipari and A. Szabo, "Effect of librational motion on fluorescence depolarization and nuclear magnetic-resonance relaxation in macromolecules and membranes," Biophys. J. **30**, 489–506 (1980).
[42]K. Kinosita, A. Ikegami, and S. Kawato, "On the wobbling-in-cone analysis of fluorescence anisotropy decay," Biophys. J. **37**, 461–464 (1982).
[43]S. Kawato and K. Kinosita, Jr., "Time-dependent absorption anisotropy and rotational diffusion of proteins in membranes," Biophys. J. **36**, 277 (1981).
[44]G. F. Schröder, U. Alexiev, and H. Grubmüller, "Simulation of fluorescence anisotropy experiments: Probing protein dynamics," Biophys. J. **89**, 3757–3770 (2005).
[45]P. L. Kramer, C. H. Giammanco, and M. D. Fayer, "Dynamics of water, methanol, and ethanol in a room temperature ionic liquid," J. Chem. Phys. **142**, 212408 (2015).
[46]H.-S. Tan, I. R. Piletic, R. E. Riter, N. E. Levinger, and M. D. Fayer, "Dynamics of water confined on a nanometer length scale in reverse micelles: Ultrafast infrared vibrational echo spectroscopy," Phys. Rev. Lett. **94**, 057405 (2005).
[47]K. Schmidt-Rohr, A. Kulik, H. Beckham, A. Ohlemacher, U. Pawelzik, C. Boeffel, and H. W. Spiess, "Molecular nature of the beta. Relaxation in poly (methyl methacrylate) investigated by multidimensional NMR," Macromolecules **27**, 4733–4745 (1994).
[48]P. Vincent, "Impact strength and mechanical losses in thermoplastics," Polymer **15**, 111–116 (1974).
[49]J. Heijboer, J. Polym. Sci. Polym. Symp. **16**(7), 3755–3763 (1968).
[50]R. Casalini and C. Roland, "Aging of a low molecular weight poly (methyl methacrylate)," J. Non-Cryst. Solids **357**, 282–285 (2011).
[51]P. O. R. Muisener, L. Clayton, J. D'Angelo, J. Harmon, A. Sikder, A. Kumar, A. Cassell, and M. Meyyappan, "Effects of gamma radiation on poly (methyl methacrylate)/single-wall nanotube composites," J. Mater. Res. **17**, 2507–2513 (2002).
[52]P. Hamm and M. T. Zanni, *Concepts and Methods of 2D Infrared Spectroscopy* (Cambridge University Press, Cambridge, New York, 2011).
[53]K. Kwak, D. E. Rosenfeld, and M. D. Fayer, "Taking apart the two-dimensional infrared vibrational echo spectra: More information and elimination of distortions," J. Chem. Phys. **128**, 204505 (2008).
[54]A. Tokmakoff, "Orientational correlation functions and polarization selectivity for nonlinear spectroscopy of isotropic media. I. Third order," J. Chem. Phys. **105**, 1–12 (1996).
[55]G. U. Bublitz and S. G. Boxer, "Stark spectroscopy: Applications in chemistry, biology, and materials science," Annu. Rev. Phys. Chem. **48**, 213–242 (1997).
[56]S. S. Andrews and S. G. Boxer, "Vibrational Stark effects of nitriles I. Methods and experimental results," J. Phys. Chem. A **104**, 11853–11863 (2000).
[57]S. G. Boxer, "Stark realities," J. Phys. Chem. B **113**, 2972–2983 (2009).
[58]R. N. Zare, *Angular Momentum* (Wiley-Interscience, 1988).
[59]D. M. Brink and G. R. Satchler, *Angular Momentum*, 2nd ed. (Oxford University Press, Oxford, 1968).
[60]D. Wallach, "Effect of internal rotation on angular correlation functions," J. Chem. Phys. **47**, 5258–5268 (1967).
[61]T. Tao, "Time-dependent fluorescence depolarization and Brownian rotational diffusion coefficients of macromolecules," Biopolymers **8**, 609–632 (1969).

[62]L. D. Favro, "Theory of the rotational Brownian motion of a free rigid body," Phys. Rev. **119**, 53–62 (1960).
[63]Wolfram Research, Inc., Mathematica, 10.0 ed., Wolfram Research, Inc., Champaign, Illinois, 2014.
[64]A. Datta, S. K. Pal, D. Mandal, and K. Bhattacharyya, "Solvation dynamics of coumarin 480 in vesicles," J. Phys. Chem. B **102**, 6114–6117 (1998).
[65]M. L. Horng, J. A. Gardecki, A. Papazyan, and M. Maroncelli, "Subpicosecond measurements of polar solvation dynamics: Coumarin 153 revisited," J. Phys. Chem. **99**, 17311–17337 (1995).
[66]N. Sarkar, A. Datta, S. Das, and K. Bhattacharyya, "Solvation dynamics of coumarin 480 in micelles," J. Phys. Chem. **100**, 15483–15486 (1996).
[67]M. Maroncelli and G. R. Fleming, "Comparison of time-resolved fluorescence Stokes shift measurements to a molecular theory of solvation dynamics," J. Chem. Phys. **89**, 875–881 (1988).
[68]M. Maroncelli, "The dynamics of solvation in polar liquids," J. Mol. Liq. **57**, 1–37 (1993).
[69]R. Kubo, M. Toda, and N. Hashitsume, *Statistical Physics II: Nonequilibrium Statistical Mechanics*, 2nd ed. (Springer, Berlin, Heidelberg, 1991).